Department of Precision and Microsystems Engineering

Reset based Skyhook damping

Mohammed Miyaji

Report no : 2021.080
Coach : Nima Karbasizadeh
Professor : Dr. S.H Hossein Nia
Specialisation : Mechatronic System Design
Type of report : Master Thesis
Date : October 25, 2021

Reset based Skyhook damping

A nonlinear control method for improved transient response.

by

Mohammed Miyaji

to obtain the degree of Master of Science

at the Department of Precision and Microsystems Engineering

Faculty of Mechanical, Maritime, and Materials Engineering (3mE)

Delft University of Technology

The Netherlands

To be defended publicly on Monday October 25, 2021 at 2:00 PM.

Student number:	5016746
Supervisor:	Dr. S.H. HosseinNia
	Nima Karbasizadeh
Thesis committee:	Dr.ir. J.F.L. Goosen
	Dr. S.H. HosseinNia
	Nima Karbasizadeh

TU Delft Delft University of Technology

To my parents Yasmin and Khojema, and my brother Mohsin.

Abstract

As the age of industry 4.0 evolves expeditiously, the demand for improved performance in the high-tech industry is rapidly increasing. Industries such as the semiconductor, optical, and metrology have a higher standard in regards of precision to enhance throughput rates and reduce production times between its various stages. The complex machines operating in such conditions are often exposed to structural or ambient vibrations, which pose a challenge to throughput rates. Hence it is a primary need to isolate the system from these vibrations by quickly damping them before it hampers the system process.

In this thesis, a novel approach to active vibration isolation using skyhook damping is undertaken by introducing a reset-based bandpass filter. This filter is used to achieve finite-time vibration isolation for a damped metrology frame, and its development is inspired by the success of switch-based control in active isolation. The effectiveness of the filter is numerically tested for multiple types of vibration disturbances for improved transient damping characteristics, These findings are compared to a linear counterpart of the filter, demonstrating the benefit of applying reset control for improving transient performance.

Preface

This preface will serve as an overview of this thesis so that readers can efficiently read the content of their choice.
Chapter 1 gives an introduction to this thesis and gives the motivation for this work based on industrial relevance.
Chapter 2 builds the foundation of the main thesis by introducing necessary concepts of active isolation, and the drawbacks of linear control, hence motivating the need for nonlinear control techniques,such as reset control.
Chapter 3 then establishes a link between the developed technique and the research objectives by identifying current gaps in the literature.
Chapter 4 is the essence of this thesis. This chapter explains the controller design and how it is generated, along with leading questions which should be considered while performing tests and simulations.
Chapter 5 discusses the results of numerical simulations performed on the proposed design, and also takes into account possible avenues for future research. Finally, Chapter 6 concluded the study and summarizes the thesis contributions, and suggesting future work that can be done with this study.
For readers who would like to retrace the steps, plots and results obtained in this study, the Appendices might be the place to go to.
Appendix A contains a google drive link to the MATLAB codes used for the simulations performed, along with simulink models required to run them.
I hope this preface helps you in understanding the contents of this document, and optimize your energy.

Mohammed Miyaji
Delft, October 2021

Acknowledgments

This thesis was made possible by the work and research being conducted at the Department of Precision and Microsystems Engineering, TU Delft. I want to thank God, the friends I made during my masters, colleagues, and my family who supported me through this journey.

I am immensely grateful for having Nima Karbasizadeh as my daily supervisor. His patience, support and encouragement in the duration of my thesis is greatly appreciated. His out-of-box thinking and critical analysis encouraged me to have a much innovative look at my research. I was also fortunate to have and Dr. Hassan HossenNia as my main supervisor. His positive attitude, enthusiasm and curiosity was an inspiration for the work presented. I am thankful to him for giving me an opportunity to pursue my thesis in the field of reset control, and having me as a part of the MSD group. The weekly Monday meetings held by Hassan, Jo Spronck and Marcin Kaczmarek were very fruitful. The discussions held in the meeting gave me an opportunity to think outside the box and gave me perspective on the challenges I faced. I would like specially thank Bardia Sharif, Marcel Heertjes, and Sef Achten from TU Eindhoven for helping me with the active isolation MATLAB codes and troubleshooting certain simulations.

I express my gratitude to my friends and peers: Mathew, Akash, Mark, Victor, Roald, Ali, Lukas, and the PME boys. The help and support you provided - be it technical discussions, mental support, or just great conversations - is deeply appreciated.

Last, but definitely not the least, I would like to thank my family and loved ones, both present and not. Your love and support is what made me reach where I am, and Insha'Allah it will take me further. The presence of my parents and my brother were a constant source of strength and motivation throughout my student years.

Contents

1 Introduction

As the world progresses further into the uncharted territory of innovation, new tools, techniques and ideas are put through rigorous trials. When successful, humanity progresses even further and the cycle repeats itself. Innovation has brought us from stones to swords, and from horses-carts to spaceflight. Today we as a species have conquered even electricity, by packaging it up into small smartphones by electronics means- which is the crux of most if not all the appliances we use today.
At this moment however, the high-tech semiconductor industry has taken a hit as there is a mass shortage of silicon chips [10], which is the essence of all electronic devices. Once the production and supply of these products start, there will be a strong sense of urgency and responsibility to fulfil this demand. In short, An increase in demand of the overall throughput production rate will be the motivation, supported by reduced production times for industrial automation.
The high tech industry uses machines such as lithographic wafer scanners and metrology systems like co-ordinate measuring machines (CMMs). From a mechanical engineer's standpoint, friction and backlash in moving systems are issues that come to mind while trying to boost throughput for machines like these. Some design modifications such as adding more compliant elements overcome these issues, and improve accuracy up to the nanometer level. This unfortunately comes at a cost of making the structure more susceptible and highly sensitive to ambient vibrations. To maintain the accuracy and performance of these machines in the precision industry, these vibrations need to settle first, which unfortunately hits the throughput rate negatively. Therefore, damping these vibrations and improving transient performance should be focused on.
Vibration isolation techniques have been used in industry to dampen these disturbances sufficiently, and the existing state-of-the-art use linear control strategies to achieve just that. However, there are certain nonlinear methods which hold potential to improve transient performance when compared to these linear techniques. The aim of this research thesis is to develop and simulate a nonlinear skyhook damping technique, which is also easy to design and tune using frequency domain analysis, and shed light on how its transient damping performance compares to its linear counterpart. This study also aims to investigate how high of a damping gain can be achieved, while ensuring stability and robustness as much as possible.

1.1. Outline

This thesis is divided in the following chapters.

- Chapter 2 provides the foundation knowledge in the form a literature survey. It covers information on vibration isolation techniques used in industry, along with an in-depth understanding of reset control - a nonlinear control method. It explains the need for a nonlinear control technique in vibration isolation.
- Chapter 3 establishes research gap and objectives, once the background and state-of-the-art has been studied.
- With the objectives clear, chapter 4 contains the main contributions of this thesis, and includes the controller design concept.

- Chapter 5 contains the numerical test results of the designed controller, and is divided based on tests conducted on individual aspects of the controller.
- Chapter 6 concludes the study, summarizing the contributions, and provides additional suggestions for future work to be done on this architecture.

2

Literature overview

This chapter acts as a review of appropriate literature and concepts, upon which this thesis is formed on. In section 2.1, the basics of different vibration isolation techniques used in industry are introduced, where the differences between passive and active damping are shown mathematically. Section 2.2 discusses the reason why linear techniques are used, and provides incentives to explore nonlinear control methods. The main focus will be on a form of sliding mode control called reset control. This section will also provide information on the tools required for frequency domain analysis of reset systems. Section 2.3 gives insight for the energy distribution and dissipation in the dynamic system where damping is introduced. This section provides reasoning for the need of nonlinear control in active isolation in the aspect of improved damping from a more mechanical perspective.

2.1. Vibration Isolation

In the field of precision mechatronics, vibration isolation becomes an important design aspect especially in the semiconductor industry. The type of isolation technique used on a system varies depending on certain factors. It can be the source of the vibration, its frequency, the mechanical design and objective of the machine, etc. Most machines in the precision industry are designed with flexible structures, therefore the disturbances can be either from ambient vibrations, or generated within the structure itself. The aim of these isolation techniques is to add damping to these structures, and are mainly classified into the following- passive, semi-active (Relaxed), and active isolation. Figure 2.1 illustrates a metrology system in the form of mass-spring system, and how the three different techniques inject damping into the system.

2.1.1. Passive Vibration Isolation

Passive vibration isolation mainly makes use of structural components such as springs and dampers to isolate the payload mass from ambient disturbances. Other well known passive elements used in industry are tuned-mass dampers, magnetic dampers etc [29] [9]. However these techniques add mass to the system and make it harder for parametric tuning of the system. This sub-section will explain aspects which influence how

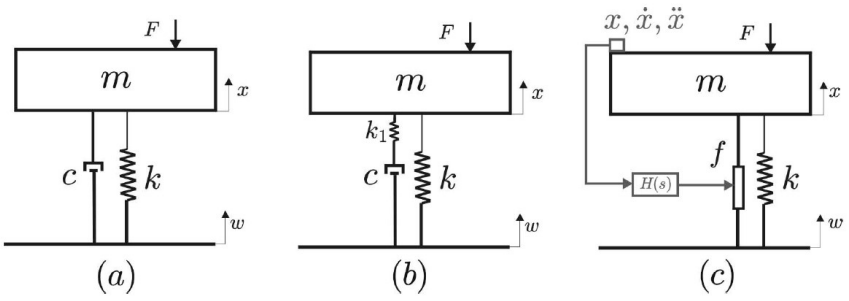

Figure 2.1: Physical representation of a) Passive isolation; b) Semi-active Isolation; c) Active Isolation achieved using controller $H(s)$ [9]

vibrations are transmitted to a payload mass, and how the passive technique can reduce its influence. A passive system is essentially modelled as a mass-spring-damper system as shown in equation 2.1a, where m is the mass of the metrology frame supported by a spring and damper of stiffness k and damping coefficient c respectively. The frame's position x is measured with respect to a certain reference, while the position of the base to which the frame is connected to is given by w. The disturbance on the mass is due to force F, which come from environmental and seismic vibrations, or through the base itself.

$$m\ddot{x} + c(\dot{x} - \dot{w}) + k(x - w) = F \tag{2.1a}$$

$$m\ddot{x} + c\dot{x} + kx = F \qquad \text{if } w = F = 0 \tag{2.1b}$$

$$\ddot{x} + 2\zeta_p \omega_n \dot{x} + \omega_n^2 x = 0 \tag{2.1c}$$

When the system is considered to be at complete rest, i.e. when $w = 0$ and $F = 0$, the differential equation of the model can be re-written as equation 2.1c. Here, $\omega_n = \sqrt{k/m}$ is the natural frequency of the system in rad/s. It is at this frequency that the system has its first rigid body resonance mode, and this is maximum amplitude of gain is achieved by the system (figure 2.2). $\zeta_p = c/(2\sqrt{k \cdot m})$ is the dimensionless passive damping ratio. It is an industry standard to use $\zeta_p = 0.7$ as a damping ratio, to obtain a favourable balance among settling time and overshoot in the transient response of the system.

$$\begin{aligned} X(s) &= \frac{cs + k}{ms^2 + cs + k} W(s) + \frac{1}{ms^2 + cs + k} F(s) \\ &= \mathscr{T}(s) W(s) + \mathscr{C}(s) F(s) \end{aligned} \tag{2.2a}$$

$$\tag{2.2b}$$

$$\mathscr{C}(s) \cdot (ms^2) + \mathscr{T}(s) = 1 \tag{2.2c}$$

Equation 2.2 shows the system in the Laplace domain and here we see two prominent transfer functions; the *transmissibility* $\mathscr{T}$(s) and the *compliance* $\mathscr{C}$(s). Transmissibility expresses the relation of how the position of the payload mass $X(s)$ is influenced by the floor vibrations $W(s)$, i.e a relation expressing the influence of disturbances being *transmitted* to the system. Compliance expresses the sensitivity of the mass to external forces F, how easily the system *complies* to external forces.
A sign of good isolation is when the transmissibility function is less than 1. Hence to increase passive isolation, the first parameter to reduce that comes to mind is the natural frequency of the system. However, doing so only increases the sensitivity of the system at lower frequencies, as shown in figure 2.2(b). Reducing the resonance peak is also desirable, which can be done by increasing the damping coefficient c. However this reduces disturbance rejection at higher frequencies, as the roll off slope has changed to -1 from -2, increasing gain in that range, as shown in figure 2.2(a). This also makes sense as at higher frequencies, a stronger damping element acts as a stiff element and transmits vibrations as a stiff spring. This is one trade-off in a passive design, between damping and isolation. Also, to reduce natural frequency the stiffness should be reduced. This inversely affects the compliance and makes the system highly sensitive to external force F. This is another trade-off occurring between isolation and robustness of the system to external forces. In conclusion, passive isolation performs poorly at lower frequencies. To overcome these trade-offs, active isolation control is used. This technique improves in minimizing the transmissibility and compliance of a vibration isolation system.

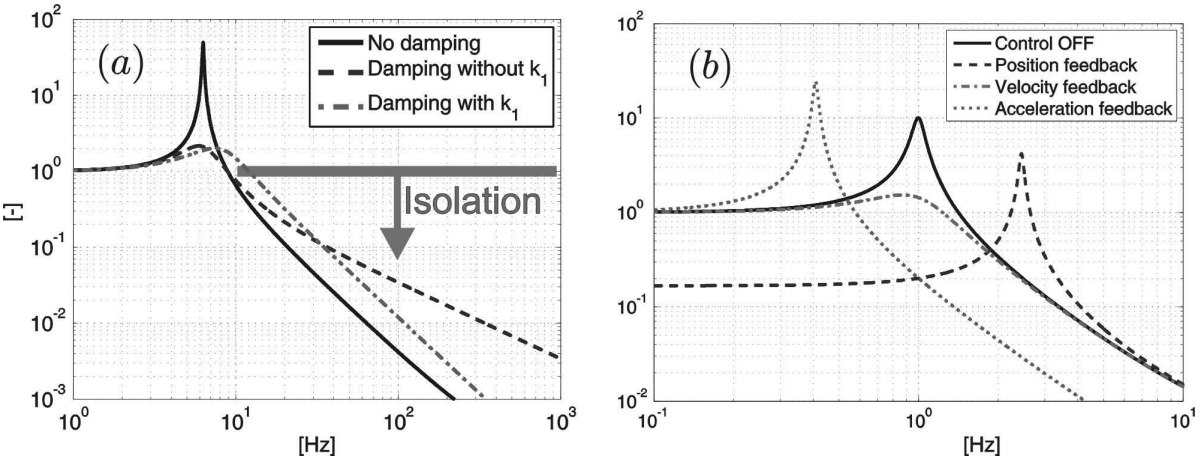

Figure 2.2: Transmissibility curves of isolation systems a) With isolators as shown in Fig. 2.1 (a) and (b); b) With isolator in Fig. 2.1 (c), [9]

2.1.2. Active Vibration Isolation

Active vibration isolation (AVI) utilize sensors and actuators to actively pump damping into the system. Using active control adds relatively little mass if actuators and sensors are wisely chosen, and the tune-ability is far easier since the control provides damping based on the position, velocity or acceleration sensor data of the payload. This technique employs use of accelerometers and other motion senors. This sensor data is fed to a controller, usually a filter which parses useful data to an actuator connected to the payload mass. This actuator then suppresses incoming vibrations by effectively dissipating the change in energy of the system. This is achieved using a combination of both feedback and feedforward control [4] in the system. However to reduce complexities in this research, only feedback control is chosen as the primary focus.

The result of the feedback control is influenced by the choice of the sensed variable. Therefore, damping of a system can be injected based on either the acceleration, velocity, or position of the payload. In the Laplace domain, forces due to inertia are equivalent to adding virtual mass. Similiarly forces due to velocity are equivalent to virtual dampers, and forces related to position are equivalent to virtual stiffness. Acceleration feedback of the metrology frame adds a virtual mass to the system which is equivalent to adding real mass in a passive system. Whereas position and velocity feedback creates a skyhook spring and damper respectively. The latter two techniques induce a force onto the system from a virtual reference of rest, as if they are connected to the "sky". Figure 2.2(b) illustrates the influence of these concepts on transmissibility. As observed, acceleration and position feedback shift the dynamics of the system globally. This research will focus on skyhook damping, since it has interesting effects in damping of suspension modes by just changing the Q factor of the resonance peaks.

2.1.3. Skyhook Damping

The concept of skyhook damping revolves around the idea of damping the system with a damper which is detached from the world. It does so by using the velocity of the frame against itself, and injecting damping into the system. The velocity data of the isolated payload is the sensed variable. This is then passed through a control unit, which usually filters the signal of noise. This filtered signal is fed to an actuator to provide the necessary damping force with damping coefficient β to the system. This results in the following transmissibility and compliance functions (equations 2.3a and 2.3c).

$$\mathscr{T}_{sky} = \frac{x}{w} = \frac{c_n s + k}{ms^2 + (\beta + c_n)s + k} \tag{2.3a}$$

$$\mathscr{C}_{sky} = \frac{x}{F_d} = \frac{1}{ms^2 + (\beta + c_n)s + k} \tag{2.3b}$$

$$\beta = 2\zeta_{active}\sqrt{k \cdot m} \tag{2.3c}$$

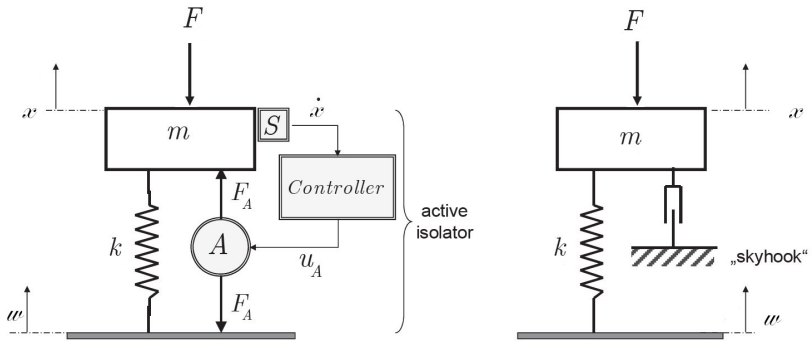

Figure 2.3: Mechanical diagram of a skyhook damping setup applied to a mass-spring system

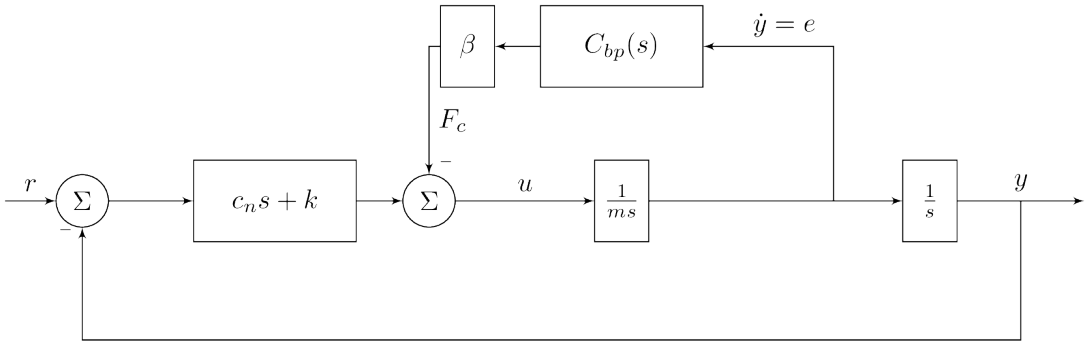

Figure 2.4: Block diagram of a skyhook damper design applied to a mass-spring-damper system

It should be noted that c_n is the natural damping of a system without the presence of any damping element. This value is quite small and makes the influence of the skyhook damping force decisively dominant. The skyhook damping coefficient β is controlled by a dimensionless active damping ratio ζ_{active}., which unlike ζ_p in passive systems, is actively tuned as a gain value in a control loop (illustrated in figure 2.4).

This influence is shown clearly in equation 2.4, which highlights the relationship of transmissibility, compliance, and β through skyhook damping force $\mathbf{C}(s)$.

$$\mathbf{C}(s) = \beta C_{bp}(s) \tag{2.4a}$$

$$\mathscr{C}_{sky}(s) \cdot (ms^2 + \mathbf{C}(s)) + \mathscr{T}_{sky}(s) = 1 \tag{2.4b}$$

As discussed earlier in section 2.1.1, minimizing the transmissibility function should be an initial goal. Equation 2.4 shows that without changing the mass, increasing the skyhook damping force $\mathbf{C}(s)$ appropriately allows precise tune-ability and control over damping the vibration modes.

2.1.4. Performance analysis

The performance analysis of any motion control system in the context of AVI is done on the basis of the following criteria [2] [3]:-

1. Time domain transient response.
2. Steady state vibration suppression. (Transmissibility)
3. Rejection of disturbances applied directly to the system. (Compliance)

The transient response of a system after motion gives information regarding how quick disturbances settle before it reaches a steady state. Two important aspects to note are the overshoot percentage and the settling

time it takes to reach steady state. In the frequency domain, performance is measured by the compliance and transmissibility functions. The phase characteristics are also taken into consideration as reduced phase lag is equivalent to a faster response in time domain.
So far the dynamics of the system have been discussed, but for an AVI system the essence of the damping is provided by the control strategy employed in the system. The next section sheds more light on control design, and possible improvements in that domain.

2.2. Control strategies for skyhook damping

In skyhook damping, the controller used are most often linear bandpass filters. This is because this one filter solves two challenges which appear in AVI systems [2][21]. It reduces firstly the garbage information picked up by accelerometers at very low frequencies, and secondly any form of spillover from high frequency noise. This helps us focus on a frequency band and attack one or at most two resonance mode of the system. However linear controllers are often held back by certain limitations. This section will introduce a nonlinear alternative called reset control.

One of the limitations of linear control is the Bode phase-gain relation, which states that any change in the phase of the system linearly changes the slope of the gain as well. It is desirable to have as much phase margin around the bandwidth frequency in the open loop, as it makes the system more robust to changes when the loop is closed. Another is the waterbed effect due to Bodes sensitivity integral. As shown in the equation 2.5, and figure 2.5, if a system excels in reference tracking at lower frequencies, it takes suffers in performance at rejecting disturbances at higher frequencies and vice versa.

$$\int_0^\infty \ln|S(j\omega)|d\omega = 0 \tag{2.5}$$

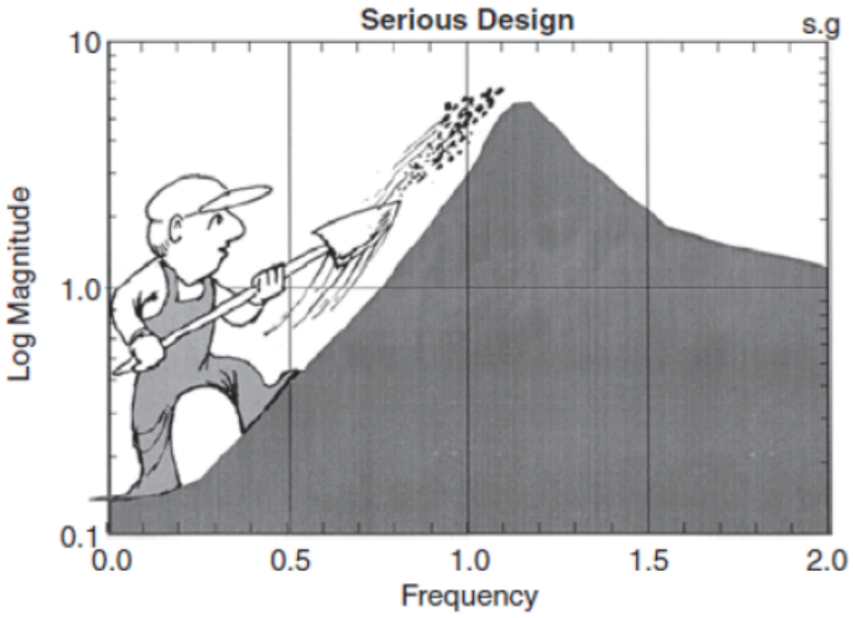

Figure 2.5: The waterbed efffect [33]

The alternative which is explored in this paper is using nonlinear control paradigms.[1] Some examples in literature of applied nonlinear control techniques are sliding mode control, switching control, adaptive unscented kalman filters, etc [11][16][28]. This study will focus on switching control methods, mainly reset control. Filters such as unscented kalman filters require lots of data along with precise design, making them difficult to design and re-tune. Switching control [18] employs the idea of switching the controller between two states on linearity and non-linearity. They are also tuned based on time based switching (occurs at a

specified time interval) or state-based switching (occurs at a particular state of the controller).
Hybrid Integrator-gain system (HIGS) is a form of sliding mode control and has been applied as a skyhook damper controller in an AVI setup in [17] and [2], where a HIGS based bandpass filter is designed. It has shown improved frequency domain response with better phase characteristics compared to its linear counterpart, along with time domain transient response.

In literature however, Reset control has shown to be superior to HIGS in the aspect of motion tracking, but disturbance rejection performance has not been explored. The following sections will introduce the concept of reset control and how it can be beneficial in AVI systems, along with some tools required to analyse reset based systems in the frequency domain.

2.2.1. Reset Control

Reset control is a form of sliding based control regulated by discrete and continuous dynamics of the system. The pioneer of this school of control strategy was J.C Clegg in 1958 [8] who attempted to reset the states of a linear integrator. The most basic of all reset elements was coined as the Clegg Integrator (CI) 2.6b.

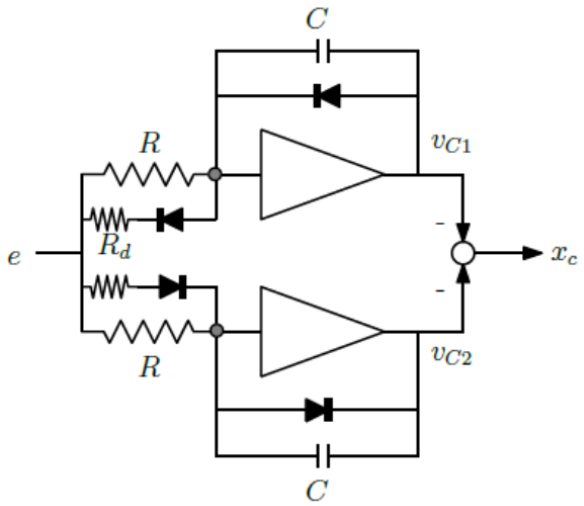

(a) Circuit of a Clegg integrator. [30]

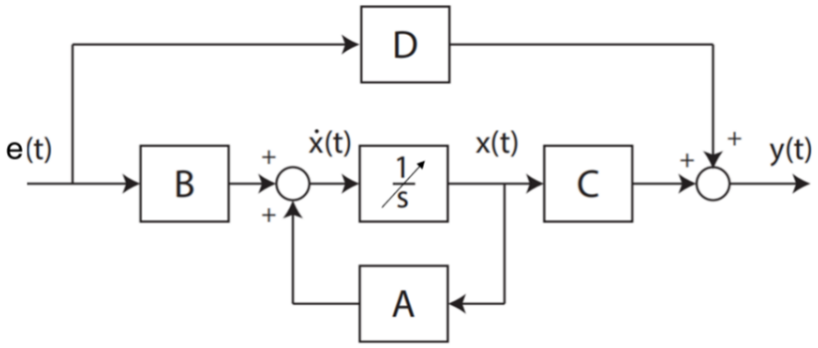

(b) State-space representation of a Clegg integrator.

Figure 2.6: Clegg integrator- Electronic and state space representation.

Reset can occur in one of two ways- either resetting the state of the integrator, or keep resetting at regular time intervals[36][15]. This thesis will focus on state based reset. The working logic is that the input and output of the controller are always of the same sign, i.e the direction of the magnitude of both is the same. It electronically it is illustrated in figure 2.6a, with equation 2.6 stating the first reset law which the design follows. The reset law states that unless the product of the input of the controller and the current state of the controller is less than or equal to 0, it operates linearly. If not, then the states of the controller are reset

to 0. This is called a zero-crossing condition (figure 2.7a). Compared to its linear counterpart, its frequency response function (figure 2.7b), shows a reduced phase lag of 38°.

$$\begin{cases} \dot{x}_c = \frac{1}{RC} e, & \text{is allowed when } x_c e > 0 \\ x_c^+ = 0, & \text{is allowed when } x_c e \leq 0 \end{cases} \tag{2.6}$$

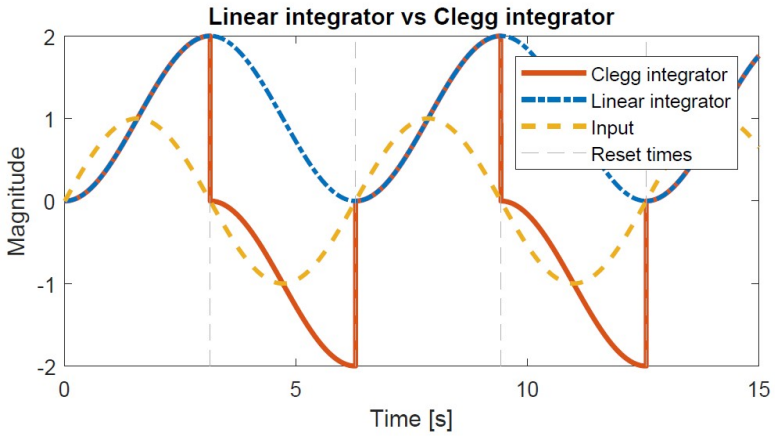

(a) Clegg Integrator (orange) showing zero crossing when the sine input (dashed yellow) crosses zero.

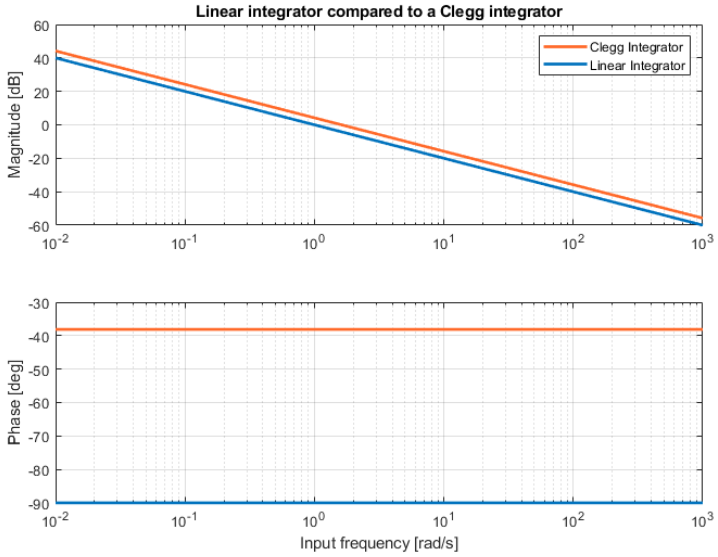

(b) Linear v/s Reset control in frequency domain.

Figure 2.7: Reset control compared to linear counterpart [19]

An open loop state space representation of a general reset system is given in equation 2.7, here x is the state vector of the open loop control system and A_ρ is a state reset matrix. This matrix determines which states of the controller are to be reset, and to what extent. When $A_\rho = 0$, full reset occurs and if $A_\rho = 1$, the controller has zero reset, and operates exactly like its linear counterpart.The rules in which the reset is designed to occur belong to a set called the flow set $\mathscr{F}$, this is where the output is that of a continuous dynamic of the reset control. The set condition where reset occurs is called as the jump set $\mathscr{J}$, and is represented by the second sub-equation in equation 2.7.

$$\begin{aligned} \dot{x}(t) &= Ax(t) + Bu(t) \qquad x,u,t \in \mathscr{F} \\ x(t^+) &= A_\rho x(t) \qquad\quad x,u,t \in \mathscr{J} \\ y(t) &= Cx(t) + Du(t) \end{aligned} \tag{2.7}$$

Over time, more improved variants of the concept were developed; as shown by Horowitz et al. who extended the idea of Clegg to a First Order Reset Element (FORE) [20] [26], which provides the advantage of filter frequency placement and has been applied for narrow band applications such as [27]. The FORE is the reset equivalent of a low-pass filter in the frequency domain. The state space matrices for a FORE with corner frequency ω_r are shown below.

$$\begin{aligned} A_r &= -\omega_r, \quad B_r = \omega_r, \\ C_r &= 1, \qquad D_r = 0, \qquad A_\rho = \gamma I \end{aligned} \tag{2.8}$$

$$\mathscr{R}(s) = \frac{1}{\frac{s}{\omega_{r\alpha}} + 1} \quad \text{with } A_\rho \tag{2.9}$$

In [13], FORE was generalised (GFORE) in a way where $A_\rho = \gamma I$. Here, gamma is an additional reset parameter and could be a value in the range of [0,1], providing a control over the nonlinearity introduced in reset. Figure 2.8, shows a a representation of how the controller behaves in the frequency domain. Note the presence of higher order harmonics, which are triggered because of the reset action. This representation is called a describing function, and is explained in detail in the next section.

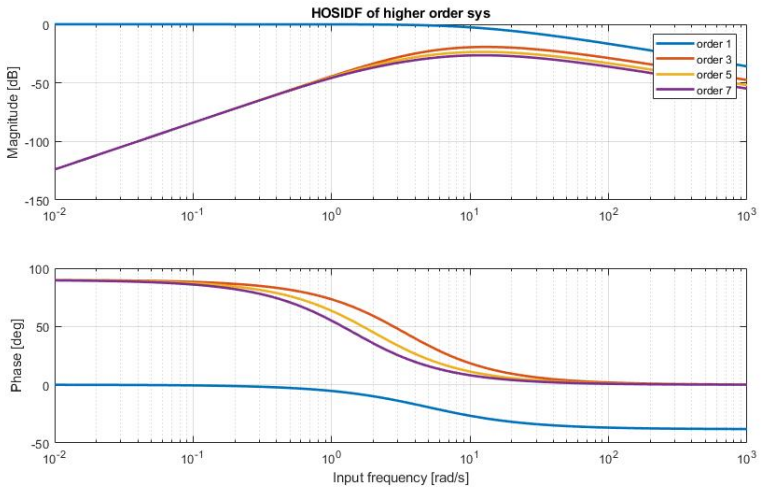

Figure 2.8: First order reset element with the presence of higher order harmonics.

2.2.2. Describing Function

Reset systems being inherently nonlinear, make it difficult to represent them in the frequency domain. Unlike linear systems which can be represented using transfer functions, nonlinear systems require alternative tools and techniques to understand frequency domain behaviour.

A linear approximation technique called describing function (DF) is used in literature for frequency domain analysis for non linear systems. It is based on quasi linearisation, which depends on the form of the input signal [35] given to the system. A sinusoidal input is usually chosen as input signal, as it similar to that of ground vibrations. Guo et al. has done an analytical calculation of a generalised reset system in [13][15][27], however it only considers the first harmonic of the Fourier series decomposition of the output, and neglects the influence of the higher order harmonics. This can result in grave inaccuracies as seen in [22]. To obtain a more accurate and reliable data about the frequency response of nonlinear systems, an appended method called “Higher Order Sinusoidal Input Describing Function” (HOSIDF) has been introduced in [19] [15][34].

For reset elements, it is defined in the following equation-

$$
\begin{aligned}
G_n(\omega) &= \begin{cases} C_r\left(j\omega I - A_r\right)^{-1}(I + j\Theta(\omega))B_r + D_r, & n = 1 \\ C_r\left(j\omega n I - A_r\right)^{-1} j\Theta(\omega)B_r, & \text{odd } n > 2 \\ 0, & \text{even } n \geq 2 \end{cases} \\
\Theta(\omega) &= -\frac{2\omega^2}{\pi}\Delta(\omega)\left[\Gamma(\omega) - \Lambda^{-1}(\omega)\right] \\
\Lambda(\omega) &= \omega^2 I + A_r^2 \\
\Delta(\omega) &= I + e^{\frac{\pi}{\omega}A_r} \\
\Delta_\rho(\omega) &= I + A_\rho e^{\frac{\pi}{\omega}A_r} \\
\Gamma(\omega) &= \Delta_\rho^{-1}(\omega)A_\rho\Delta(\omega)\Lambda^{-1}(\omega)
\end{aligned}
\tag{2.10}
$$

where $G_n(\omega)$ is the n^{th} order harmonic for a sinusoidal input of frequency ω.

2.2.3. Stability

In linear control systems, the BIBO stability is checked using frequency domain tools such as Nyquist or bode plots. For a reset controller however, to have asymptotic stability in a closed loop, the following condition must be satisfied [5] [14].It follows the principle of energy dissipation over time. For a reset system, the base linear system should be BIBO stable as an initial condition to stability.

Theorem 2.2.1 (Stability theorem) *There exists a constant $\beta \in \mathscr{R}^{n_r x 1}$ and positive definite matrix $P_\rho \in \mathscr{R}^{n_r x n_r}$, such that the restricted Lyapunov equation*

$$P > 0, A_{cl}^T P + P A_{cl} < 0 \tag{2.11}$$

$$B_0^T P = C_0 \tag{2.12}$$

has a solution for P, where C_0 and B_0 are defined by

$$C_0 = \begin{bmatrix} \beta C_p & 0_{n_r x n_r} & P_\rho \end{bmatrix}, B_0 = \begin{bmatrix} 0_{n_r x n_r} \\ 0_{n_{nr} x n_r} \\ I_{n_{nr}} \end{bmatrix} A_\rho^T P_\rho A_\rho - P_\rho \leq 0 \tag{2.13}$$

where A_{cl} is a closed loop A-matrix, n_r is the number of states being reset, n_{nr} being the number of nonresetting states and n_p is the states for the plant. A_p, B_p, C_p, D_p are the state space matrices of the plant.

2.3. Energy Dissipation in AVI damping

Figure 2.9 shows a control loop block diagram commonly used in mechatronics design. Here, r is the reference that is usually traced in motion control systems, and d is the disturbances that come into the system. This section focuses mainly on the energy dissipation when damping is injected into the system, and answers the question - When disturbances occur, where does the extra energy introduced into the system go?

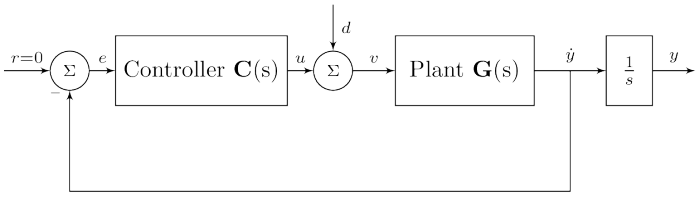

Figure 2.9: Block diagram of a skyhook damping motion control system. No reference is added as it is focusing strictly on disturbance rejection

When a mass-spring system is in motion, the energy of the system is either in the mass as kinetic energy, or in the springs as potential energy. Ideally if there is no damping, an oscillating system would oscillate forever. However in nature, damping is always present and a system when excited eventually comes to rest. Therefore damping elements are the energy sinks of the system, which dissipate energy through various means (heat or transferring it through fluids).
A skyhook damper dissipates energy through introducing an opposite force through an actuator. Figure 2.10 illustrates a block diagram of a skyhook damper, and how it adds a force in the direction opposite to that of motion, and hence dissipating energy.

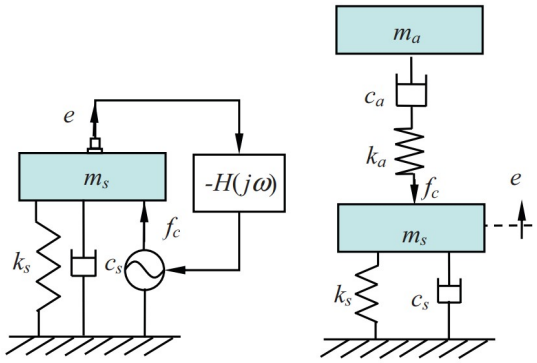

Figure 2.10: Skyhook damping illustrated along with its emulated force equivalent diagram on the right [25]

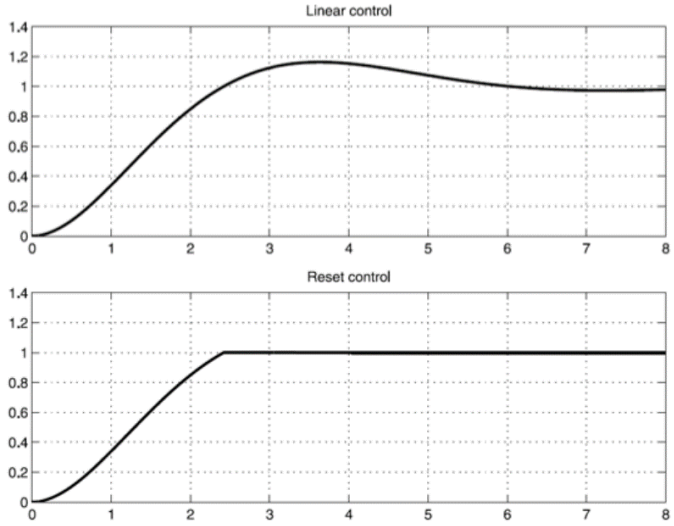

Figure 2.11: Step response of a system using linear damping as compared to reset based damping [14]

Using Reset control, real-time energy dissipation is shown in [14] and is illustrated in figure 2.11. As shown, the overshoot is theoretically zero. This is explained individually in [6] [7], where reset control is used to ideally extract energy when velocity is 0 i.e when motion of the mass is stationary. This reset technique is called an virtual absorber, and uses time based reset control to achieve finite time vibration suppression as shown in figure 2.10. This technique has not been explored using state based reset, which considers the state of the controller at each time interval of the system.

3

Gaps in Research and Objectives

3.1. Problem Definition

In chapter 2 the current state-of-the-art in skyhook damping is covered, along with control techniques used in vibration isolation. The drawbacks of passive isolation techniques are explained and the limitations of linear control in active isolation is also observed.
Reset control is a viable alternative to linear control with its operating principle, along with the ability to be designed in the frequency domain using DF. In literature it is extensively found that reset exceeds in motion tracking control, however disturbance rejection is still in theoretical stages. It is observed that time based reset techniques have achieved vibration isolation[6] [7] [15], however it is more difficult tune as it is designed in the time domain. Therefore an easier frequency domain based tuning is yet to be achieved. The tools of DF can be used for optimal control synthesis, which can also be an easier tuning alternative, similar to loop shaping techniques in linear control.
In [17] a HIGS bandpass filter is used to successfully improve transient response for step motion vibrations. It is observed that higher control gains can be implemented without triggering actuator saturation and also have improved damping at the same time. This controller is designed in the frequency domain using DF's, however no such studies have been performed using reset control.
Therefore, this instigates the question: **how would a reset based controller perform when designed for skyhook damping**. This thesis shall focus on this question and will aim to fill in the following **gaps in literature** of the state-of-the-art:

- Linear control strategies are limited by Bode's phase-gin relationship and the waterbed effect. This limits the transient damping performance that is achieved in damping.
- Reset elements are good at reference tracking [31] [23], however, disturbance rejection has not been explored using reset control. They have been theoretically studied, but have not been numerically or experimentally tested.
- Most nonlinear control techniques are not designed in the frequency domain, what most of industry has become comfortable with. Designing robust controllers troubleshooting becomes difficult if not designed in the frequency domain.

These gaps then help in stating the upcoming **research objectives** of this thesis, and are stated as follows:

- Develop a reset based skyhook damper for improved transient response when compared to a linear controller.
- The controller should be designed and tuned in the frequency domain.
- The controller performance should be validated using different types of disturbances (step, impulse, sinusoidal). The performance using various control gains which influences damping, should also be considered.

4

Reset based Skyhook Damping : Active isolation using nonlinear control

4.1. Controller Design Concept

This chapter will forge the essence of a resetting skyhook damper, by building on the concepts introduced in chapter 2. Reset controllers designed for disturbance rejection have not been studied extensively. Due to that reason, this paper will scratch the surface on initial simulation tests of the proposed design, and closed loop analysis of the controller will be studied.
Skyhook damping is often designed using a bandpass filter. Since the filter has velocity as the input variable, the reset law considers the zero-crossing of the velocity of the payload, i.e when the mass is at rest. At that moment, most if not all of the kinetic energy of the mass is stored as potential energy in the spring and the skyhook damper. Resetting the states of the controller at that instant dissipates the potential energy by injecting damping into the system.

4.1.1. Resetting bandpass filter

Before presenting the resetting bandpass filter $\mathscr{R}_{bp}$, consider the transfer function of the following linear bandpass filter $\mathscr{C}_{lin}$:

$$\mathscr{C}_{lin}(s) = \frac{u(s)}{e(s)} = \underbrace{\frac{\omega_l}{s+\omega_l}}_{\text{lowpass filter}} \cdot \overbrace{\frac{s}{s+\omega_h}}^{\text{highpass filter}}, \tag{4.1}$$

where ω_l and ω_h are the lowpass and highpass frequencies respectively, with $\omega_l > \omega_h > 0$. As observed in equation 4.1, the highpass filter adds a zero to the transfer function. This causes a problem in DF analysis using the algorithm being used by [14]. The alternatives are either using time based reset over state based [36], or creating the controller strictly using reset elements with low-pass characteristics. The latter choice is explored in this paper, using basic reset elements which are more commonly used.
This thesis tests two FOREs in combination to form a bandpass filter. FOREs are extensively studied and used in reset literature and are easier to work with in state-space implementations. This reduces sources of errors and uncertainties in the design and makes it easier to work with. To form the bandpass, the FOREs are subtracted with each other as shown in figure 4.1.

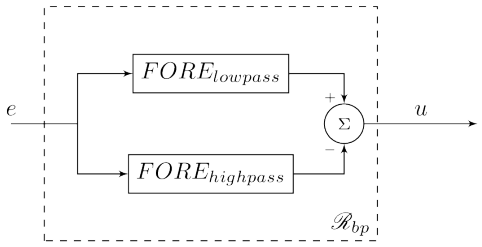

Figure 4.1: FORE's of two different corner frequencies subtracted to form a bandpass filter.

Equation 4.2 shows mathematically how two FOREs of corner frequencies $\omega_{lr} = \omega_l$ and $\omega_{hr} = \omega_h$ respectively, combine to become a bandpass filter when $A_\rho = \gamma = 1$ (no reset). It is clear that the numerator is not the same as that of equation 4.1, this can be compensated by normalizing the overall gain of the controller by adding a gain of G_n.

$$
\begin{aligned}
&\text{when } A_\rho = 1,\\
&\mathscr{R}_{bp}(s) = \frac{\omega_l}{s+\omega_l} - \frac{\omega_h}{s+\omega_h}\\
&\qquad = \frac{(\omega_l - \omega_h)}{s+\omega_l} \cdot \frac{s}{s+\omega_h}\\
&\qquad = \frac{G_n}{s+\omega_l} \cdot \frac{s}{s+\omega_h}\\
&\text{when } A_\rho = 0,\\
&\mathscr{R}_{bp}(s) = \frac{\omega_l}{s+\omega_l}^{A_\rho} - \frac{\omega_h}{s+\omega_h}^{A_\rho}\\
&\qquad = G_n \cdot \frac{1}{s+\omega_l}^{A_\rho} \cdot \frac{s}{s+\omega_h}^{A_\rho}
\end{aligned}
\tag{4.2}
$$

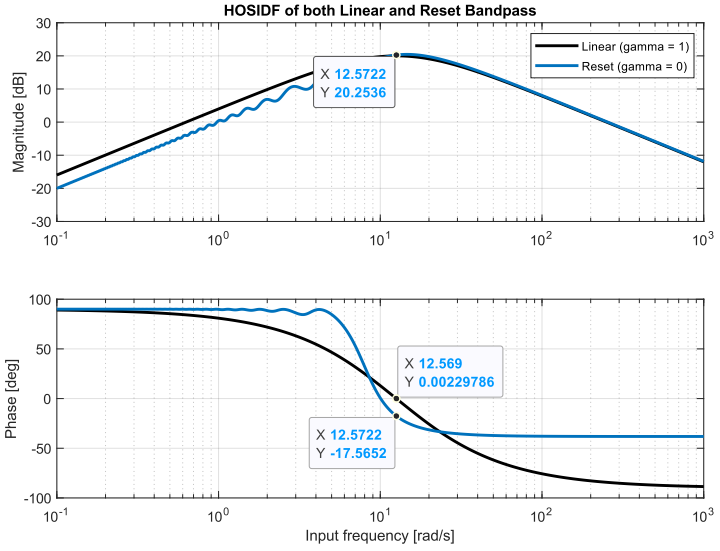

Figure 4.2: Reset bandpass filter with full reset v/s no reset

To test this architecture in a simple manner, a single resonance mode is attacked. Hence a bandpass filter is designed for a plant of resonance frequency of 12.57 rad/s (2Hz). The describing function of this element when $\gamma = 1$(no reset) and $\gamma = 0$(full reset), is shown in figure 4.2. For $\gamma = 1$, the phase lag is 0 at the resonance frequency. This makes sense as the behaviour is exactly the same as a linear bandpass filter. However at $\gamma = 0$ a phase lag of about 17 degrees is present. This means that for a reset based filter to work in this setup, a phase lag of around 17 degrees should be present after reset at the resonance frequency. This statement will also be put to the test in the numerical experiments.

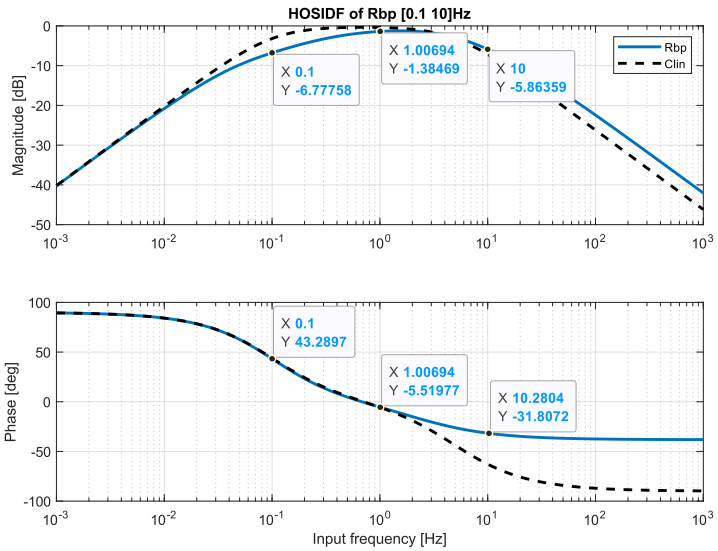

Figure 4.3: Reset bandpass filter spanning over two decades from 0.1Hz to 10Hz

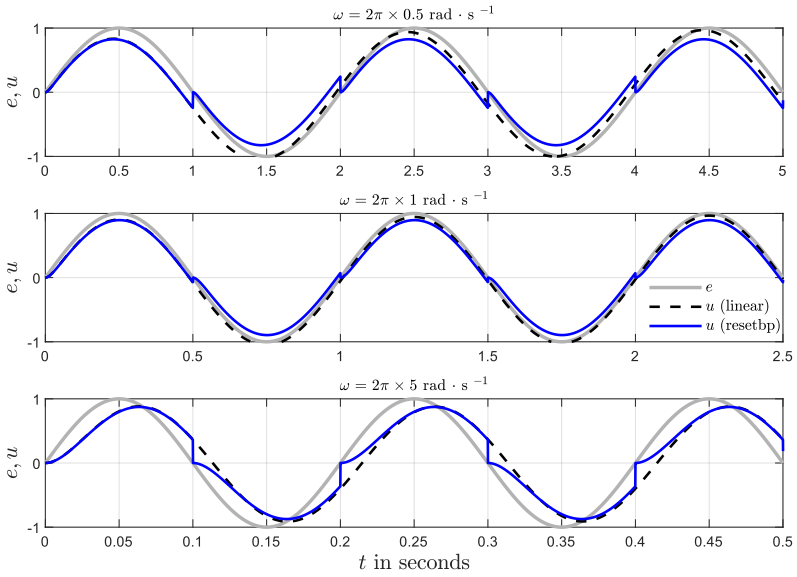

Figure 4.4: Time series simulation of the reset bandpass filter (blue) as compared to a linear bandpass filter (dashed black) from 4.3 when a sinusoidal input is given (gray).

Figure 4.3 shows an example of the $\mathscr{R}_{bp}$ filter spanning two decades. For this controller to function effectively after reset, the controller should be used for a plant with a resonance frequency of around 5Hz, where appropriate phase lag is present. Figure 4.4 shows how the controllers would perform to a sinusoidal input,

with reset occurring at the inputs zero-crossing. It can be seen that at frequencies 1Hz the significance of the resets is minimal, as the linear counterpart performs equally well as compared to $\mathscr{R}_{bp}$. At 0.5Hz, there is a phase lead in the system and it is seen that at the instance of reset, there is slightly more gain than the input amplitude; whereas at 5Hz, there is significant reset action but there is no increase in the amplitude of the controller output at the instance of reset.

4.2. Numerical Analysis and Simulations

The $\mathscr{R}_{bp}$ control architecture is put to the test by tuning it to a pre-determined plant, a metrology table provided by ASML at TU/e. The plant parameters are taken from the system identification data presented in [3]. The metrology stage is designed such that it has isolation modules for multi-axis vibration suppression. Only one axis will be focused on in this thesis, and the numerical values for the plant parameters are as follows : $m = 1300$ kg,$k = 170$ kN/m,$c = 1100$ Ns/m, which comes down to a dimensionless passive damping ratio of $\zeta_p = c/(2\sqrt{k \cdot m}) = 0.03$. Therefore the resonance frequency of the first mode of the system is at 1.8Hz.

Figure 4.5 shows the frequency response function (FRF) of the plant through system identification. It is observed that at higher frequencies there are additional resonance peaks due to higher modes of the system, and at lower frequencies, the data is unreliable due to accelerometer noise. [3] mentions that the phase of the system starts deteriorating beyond 10Hz and this is due to delay present in the Lorentz actuators used.

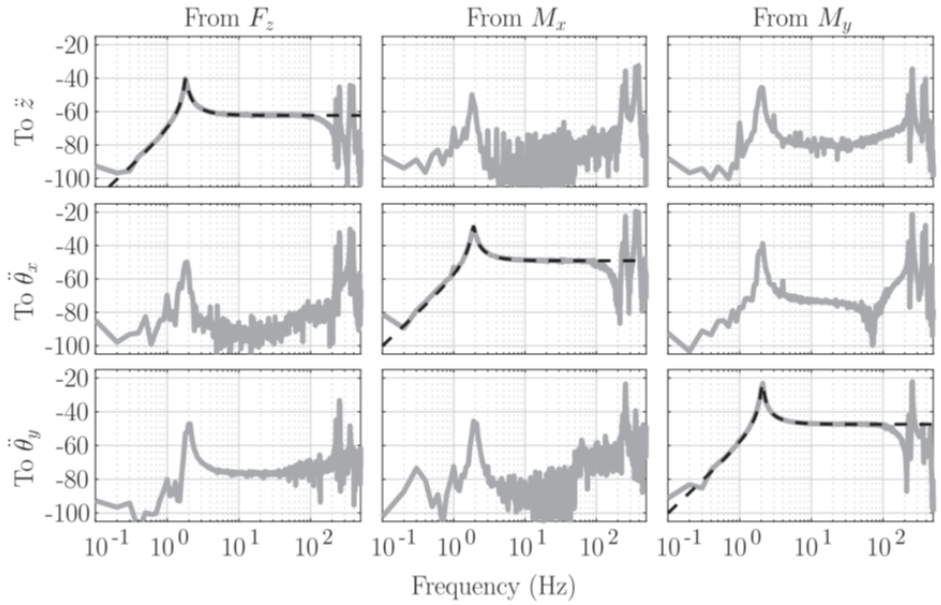

Figure 4.5: The Bode magnitude plots showing the FRFs of the measured (solid grey) and modeled (dashed black) data of the compliance of the metrology table. [3]

For a model such as this, the $\mathscr{R}_{bp}$ filter is tuned to have a band between 0.1Hz to 3Hz. For a comparative study, a linear bandpass filter $\mathscr{C}_{lin}$ is designed with the transfer function shown in equation 4.3. As illustrated in figure 4.6, at the 1.8Hz the gain for $\mathscr{R}_{bp}$ is -2.36dB and a phase lag of 19.63 degrees. This gain is normalized to with the linear gain at this frequency to ensure similar control force and to compare control performance effectively. For that, $G_n = 0.762$.

$$\mathscr{C}_{lin}(s) = \frac{G_n}{s+\omega_l} \cdot \frac{s}{s+\omega_h} \tag{4.3}$$

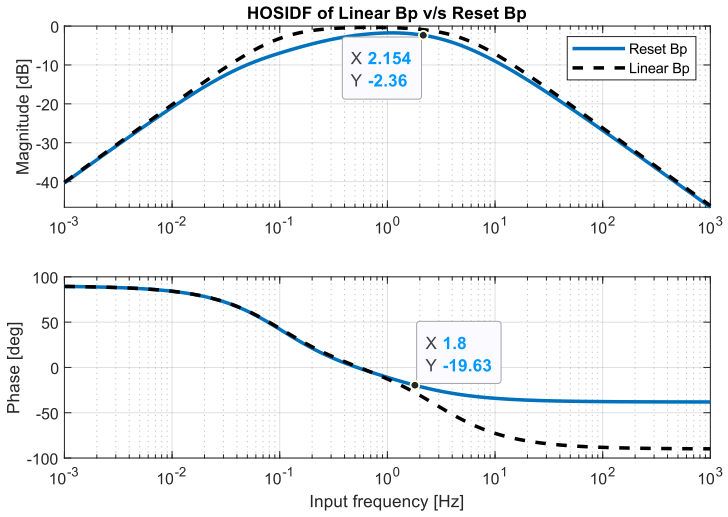

Figure 4.6: Designed $\mathscr{R}_{bp}$ filter (blue) and linear filter (dashed black) of frequency range 0.1Hz to 3Hz.

The next chapter will discuss the results of numerically testing this controller when a step, impulse or sinusoidal disturbance is imparted on the system. The influence of phase lag is also studied, along with a simplified approximation of the process sensitivity function of the closed loop.

5

Results of numerical simulation and Discussion

The performance of the designed $\mathscr{R}_{bp}$ is numerically tested using a SIMULINK model of the plant. Damping performance of the controller is studied by varying the dimensionless active damping gain $\zeta_{active} \in \{0.5, 0.7, 1, 10\}$. The results are compared to an equivalent linear bandpass filter $\mathscr{C}_{lin}$.

The figures of merit, as discussed in section 2.1, that are used to compare the performance of the two controllers are the transient response characteristics- **overshoot percentage and settling time**. For the same gains, performance will be studied for 3 separate disturbances to the system- Step, impulse and sinusoidal. The step response is used to obtain overshoot and settling time data, and the impulse and sinusoidal response are tested because these occur most if not always in practical situations.

This chapter is divided in 4 subsections. Section 5.1 discusses the simulation results of a step and impulse response. Section 5.2 discusses the simulation result of a sine disturbance. Section 5.3 discusses the questions the requirement of a phase lag for the reset system to work for varying gains. Section 5.4 expands on a particular finding in section 5.1, which is a behaviour the controller has at higher damping gains.

5.1. Step and impulse disturbance response

Figures 5.1 and 5.2 show the step responses of the system, which reaches a steady state of 5.881e−8m. Figures 5.4 and 5.5 show the impulse response. Since a pure impulse is difficult to generate, two step responses in opposite directions are subtracted from each other in a very short instance of time. The time instance is arbitrarily selected to be 0.02 seconds. For both disturbance types, it should be noted that the reset action for $\mathscr{R}_{bp}$ occurs when the velocity of the sytem reaches zero. In the position aspect,this occurs when the slope of the plot is parallel to the x-axes, i.e when the slope is zero, indicating no change in position.

In the step response for $\zeta_{active} = 0.5$, the overshoot of the system for both control strategies is the same. However at such a low active damping gain, the disturbance settles quicker for the reset based $\mathscr{R}_{bp}$, than the linear counterpart $\mathscr{C}_{lin}$. However as gains are increased, say at $\zeta_{active} = 0.7$, the reset-based bandpass filter $\mathscr{R}_{bp}$ shows a reduction in settling time by 70.33% (over 3 times faster) when compared to its linear counterpart for a step response (shown in table 1). It is observed that for $\zeta_{active} \in [1\,5]$, the performance deteriorates. This can be seen in figure 5.3, showing the percentage overshoot and settling times achieved over a set of active gains $\zeta_{active} \in [0.1\,10]$ to a step disturbance response. This is most likely due to some computational error within the simulations algorithm, or how the describing function calculates the closest approximation of the first order harmonic of the controller. After $\zeta_{active} = 5$ the overshoot performance improves again.

For the impulse response, the max overshoot for both control strategies is the same, unlike that of a step response where the overshoot gradually reduces as ζ_{active} increases. This proves a good metric of comparison for settling times. For $\zeta_{active} = 0.7$ an improvement of 49% in settling time is observed compared to its linear counterpart (about twice as fast) and is tabulated in table 2.

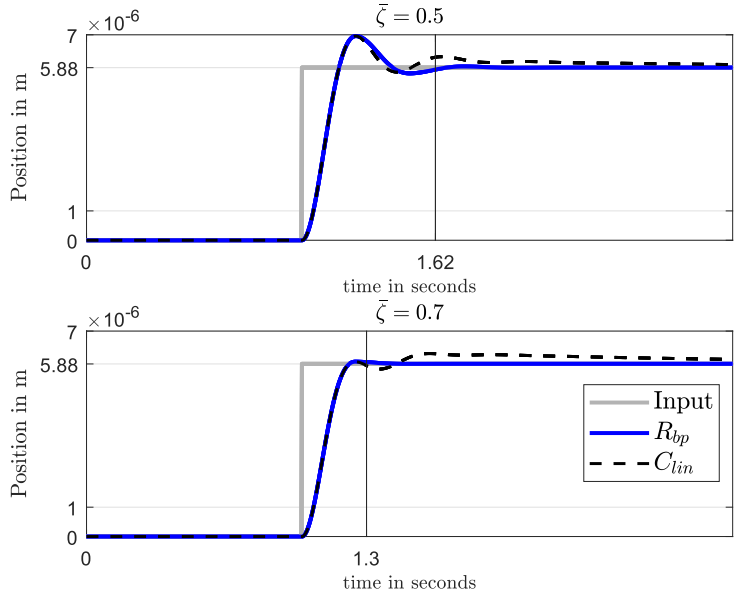

Figure 5.1: Step response of $\mathscr{R}_{bp}$ for a dimensionless active gain ζ_{active} 0.5 and 0.7 respectively. Their settling times (1.62 seconds and 1.3 seconds) and steady state values (both 5.88e-8 m) are shown in their respective axes.

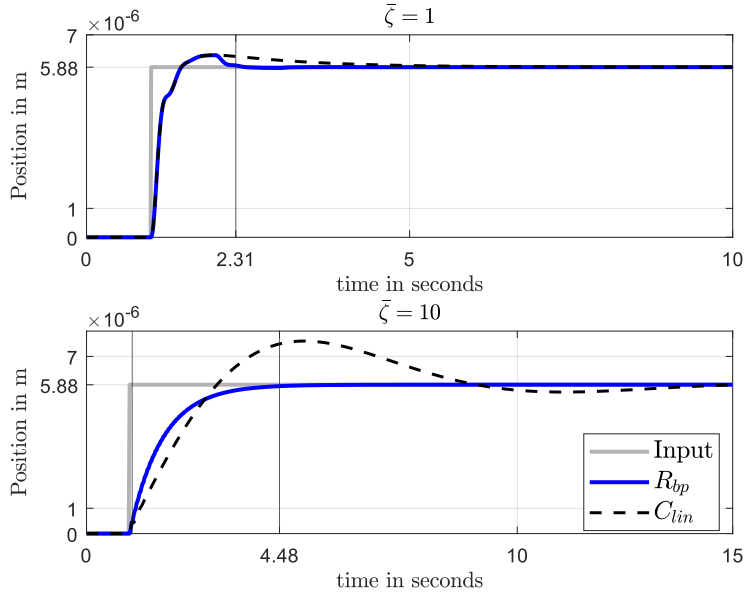

Figure 5.2: Step response of $\mathscr{R}_{bp}$ for a dimensionless active gain ζ_{active} 1 and 10 respectively. Their settling times (2.31 seconds and 4.48 seconds) and steady state values (both 5.88e-8 m) are shown in their respective axes

Table 1: Settling time performance for a step disturbance

ζ_{active}	Settling time (Linear) (sec)	Settling time (Reset) (sec)	Reduction in time (%)	Improvement in damping
0.5	3.84	1.62	57.65	2.36
0.7	4.38	1.3	70.33	3.36
1	4.94	2.31	53.29	2.14
10	14.21	4.48	68.5	3.17

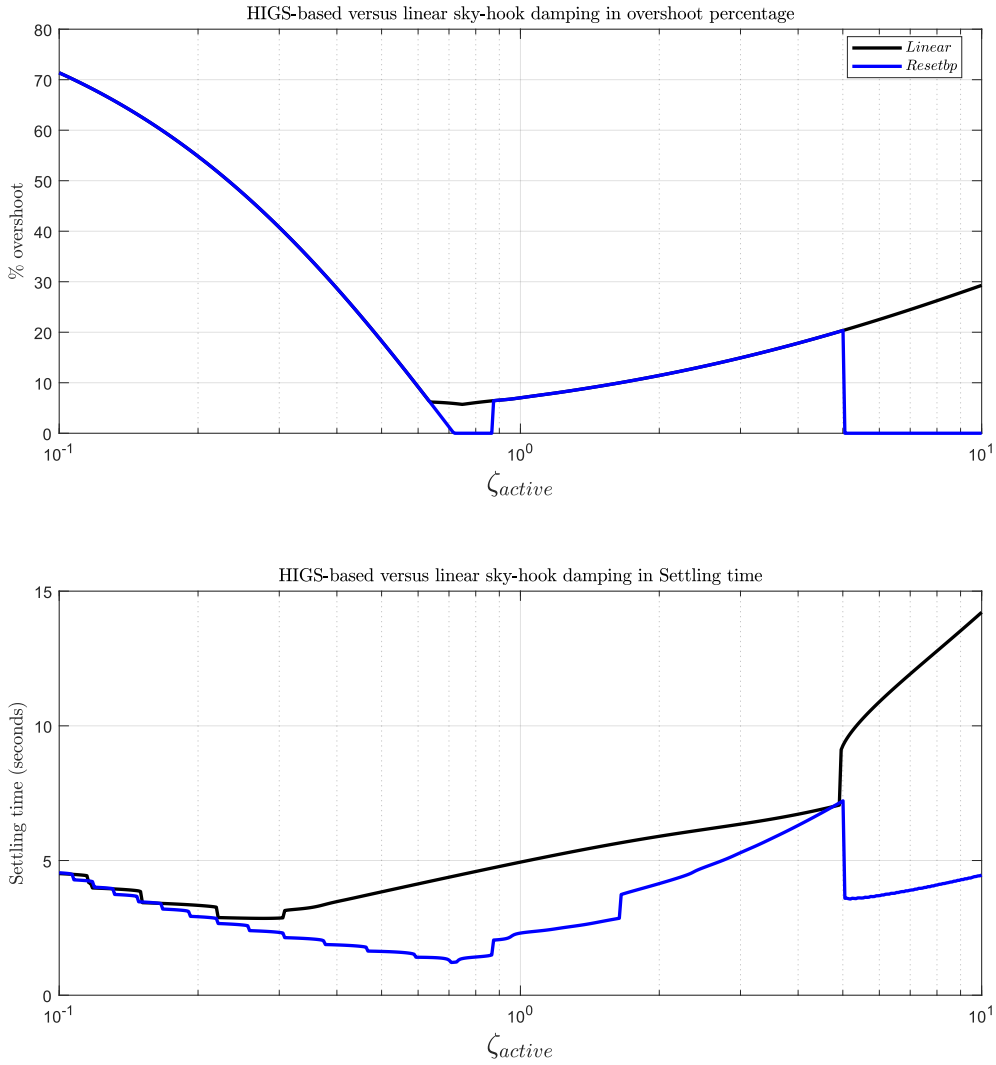

Figure 5.3: Percentage overshoot and settling time for a set of active gains $\zeta_{active} \in [0.1\ 10]$. Computational error is noticed from gains 1 to 5, and it should be assumed that in actual implementation the curve follows at a lower value.

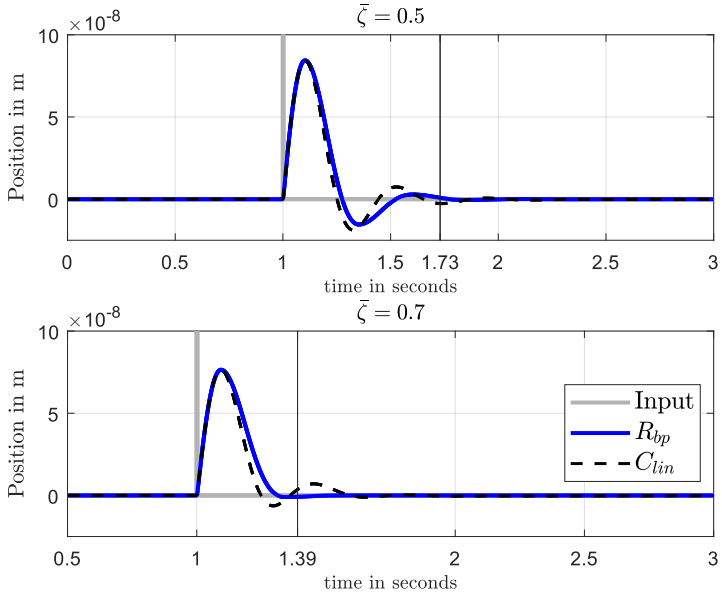

Figure 5.4: Impulse response of $\mathscr{R}_{bp}$ for a dimensionless active gain ζ_{active} 0.5 and 0.7 respectively, along with their settling times (1.73 seconds and 1.39 seconds)

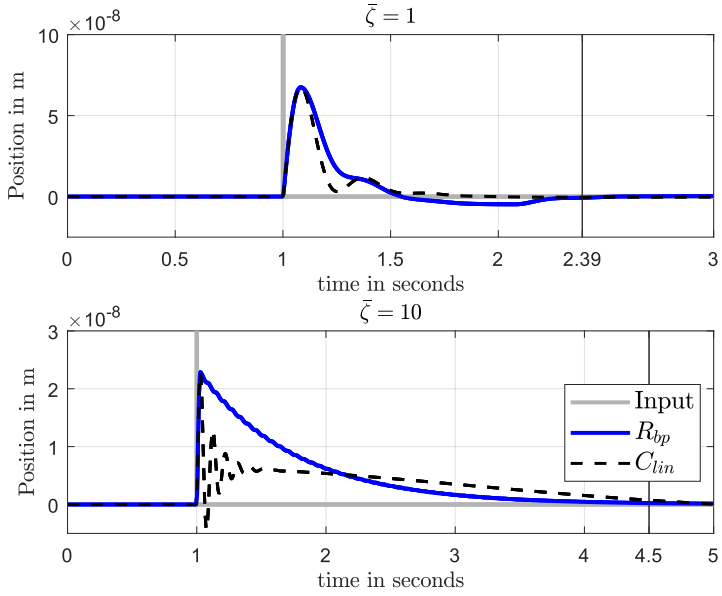

Figure 5.5: Impulse response of $\mathscr{R}_{bp}$ for a dimensionless active gain ζ_{active} 1 and 10 respectively, along with their settling times (2.39 seconds and 4.5 seconds)

Table 2: Settling time performance for an impulse disturbance

ζ_{active}	Settling time (Linear) (sec)	Settling time (Reset) (sec)	Reduction in time (%)	Improvement in damping
0.5	2.2	1.73	23.48	1.27
0.7	2.7	1.39	49.08	1.94
1	3.6	2.39	33.65	1.5
10	15.6	4.5	71.17	3.46

5.2. Sinusoidal disturbance response

A sinusoidal disturbance of the same frequency as the resonance frequency of the plant (1.8Hz). The disturbance is kept on for an arbitrary amount of time (14.8 seconds for this case) so that it achieves a steady state motion. The disturbance is then switched off and transient response is studied. Figures 5.6 and 5.7 show the results of this simulation. Table 3 shows the settling time performance to such a disturbance, and a clear improvement in settling time (close to 76% reduction for $\zeta_{active} = 0.7$).

Table 3: Settling time performance for a sinusoidal disturbance

ζ_{active}	Settling time (Linear) (sec)	Settling time (Reset) (sec)	Reduction in time (%)	Improvement in damping
0.5	0.88	0.63	23.84	1.41
0.7	1.36	0.31	76.59	4.27
1	1.82	0.4	77.78	4.5
10	13.32	1.75	86.86	7.61

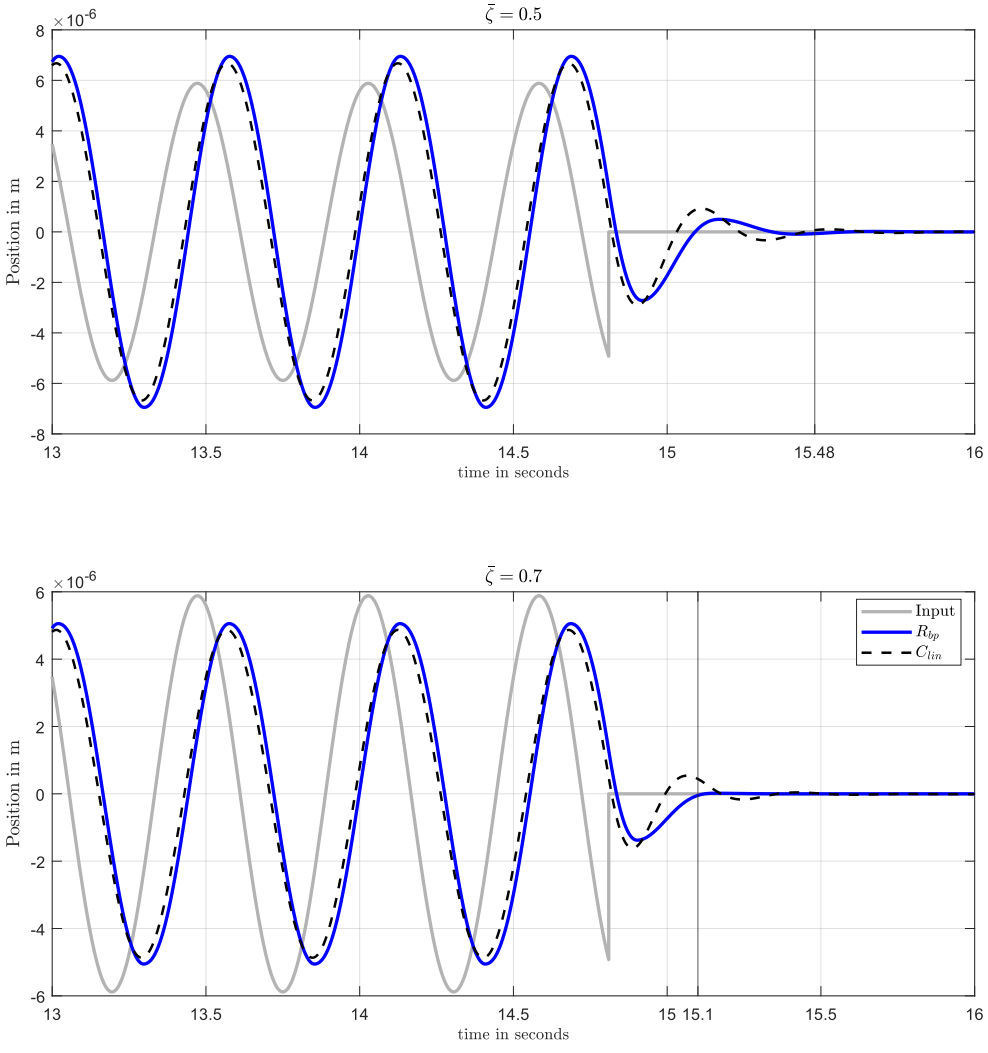

Figure 5.6: Sinusoidal disturbance response (stopping at 14.8 seconds) of $\mathscr{R}_{bp}$ for a dimensionless active gain ζ_{active} 0.5 and 0.7 respectively. Their settling times (within 0.68 seconds and 0.3 seconds respectively).

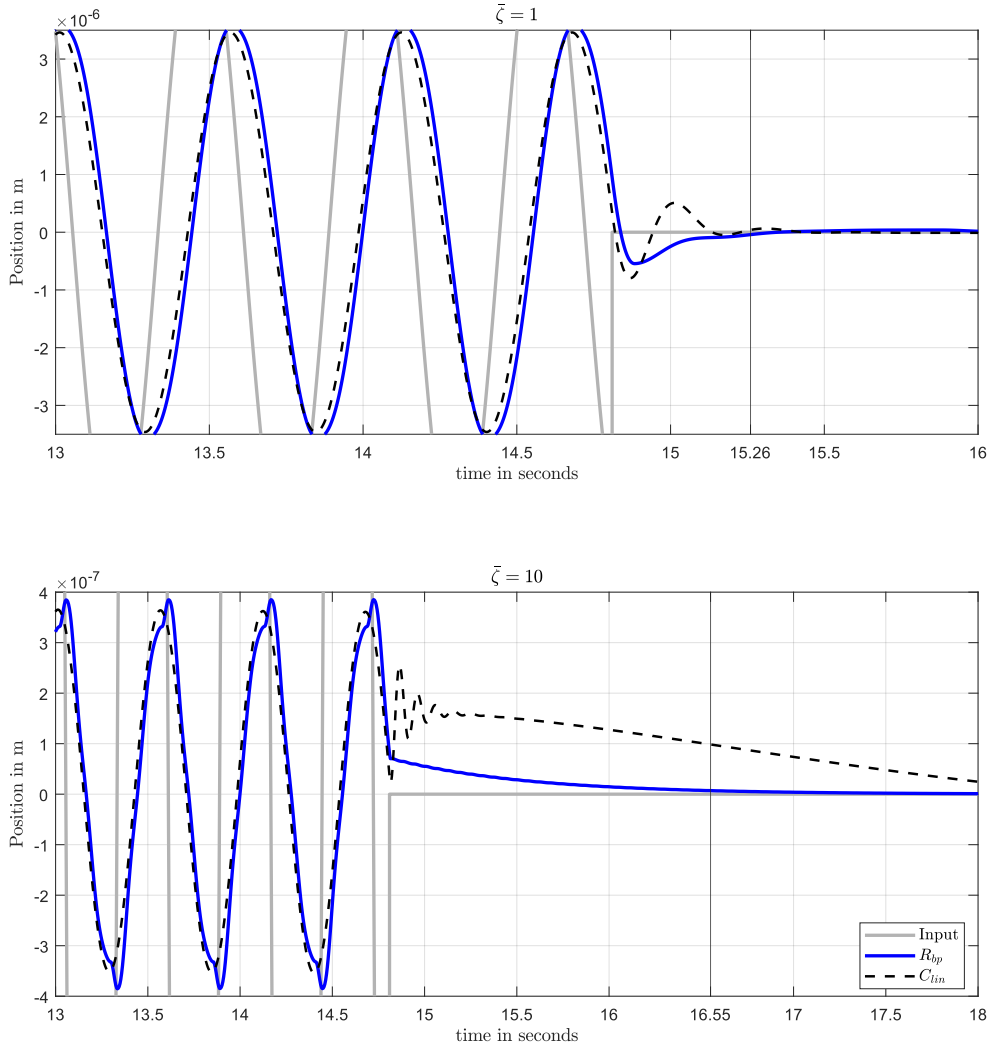

Figure 5.7: Sinusoidal disturbance response (stopping at 14.8 seconds) of $\mathscr{R}_{bp}$ for a dimensionless active gain ζ_{active} 1 and 10 respectively. Their settling times (within 0.46 seconds and 1.75 seconds respectively).

5.3. The influence of phase lag on the performance of the reset controller

The interesting point observed in $\mathscr{R}_{bp}$ is that for it to operate at its best, there should be a phase lag present at the resonance frequency. This phase lag should also be generated completely by the resetting action, and not externally induced by other controllers. However for a linear controller, phase should be zero at the resonance frequency. The amount of phase lag produced by the filter also varies with how wide the band of the bandpass designed. In chapter 4, it was found that when designed for just one resonance frequency, the designed bandpass is that of a peak. This gives us - of phase lag. When the band is widened to a decade with the resonance frequency at the centre, - of phase lag is observed.

This brings up the following questions-

- **Does the performance improve with any value of phase difference? Can a similar improvement occur in the presence of a phase lead?**
- **Does the same improvement occur with a phase difference greater than the calculated value of -19 degrees? How much of phase lag is enough? Does more mean better performance?**

To answer these questions, $\mathscr{R}_{bp}$ controller will be kept constant, and the natural frequency of the plant will be shifted throughout the bandpass range, i.e [0.1 3]Hz. This can be considered as using a de-tuned controller on systems with different natural frequencies. This way the sensitivity of the controller can be tested against plant uncertainties. Note that the transient response after a step input is observed, therefore the overshoot percentage and settling times will be the performance testing criteria.

Figure 5.8 shows the $\mathscr{R}_{bp}$ bandpass range of 0.1 to 3Hz, with a phase lead from 43 to 0 degrees in the range of 0.1Hz to 0.5Hz, and phase lag from 0 to -25.8 degrees in the range of 0.5Hz to 3Hz. Therefore, for each frequency there is a particular degree of phase that the controller has. If a plant resonance frequency is at 3Hz, it will experience a phase lag of of -25.8 degrees, an so on. The gains are normalized for each frequency tested for a fair comparison

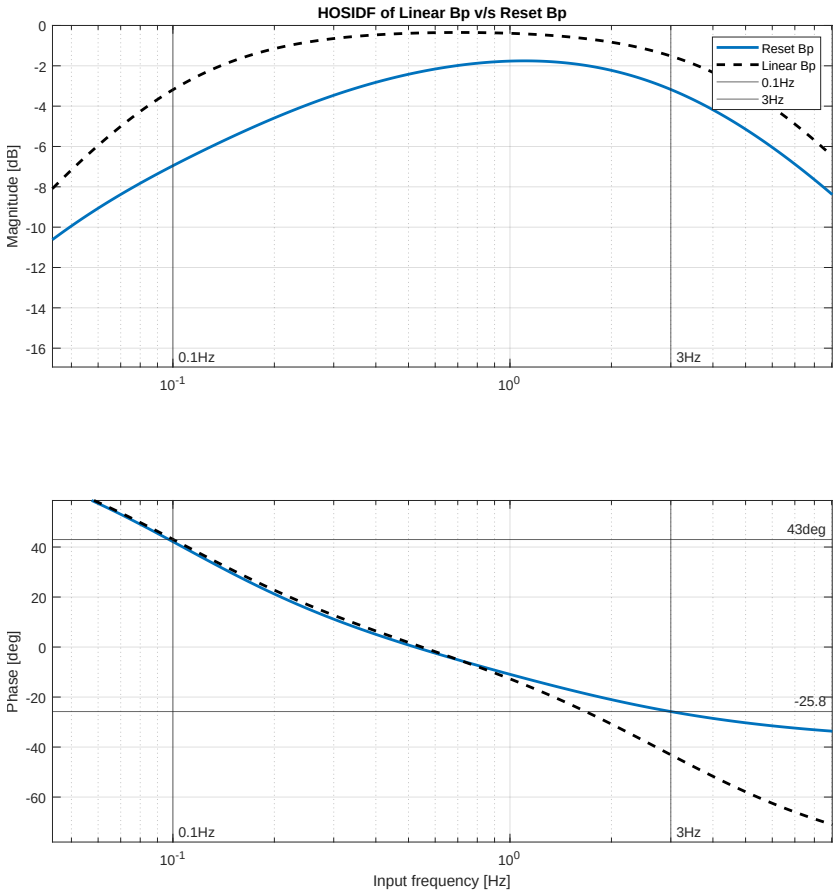

Figure 5.8: Designed $\mathscr{R}_{bp}$ filter (blue) and linear filter (dashed black) of frequency range 0.1Hz to 3Hz. This figure focuses on the area where phase difference ranges from 43 degrees to -25.8 degrees, the range of phase experienced in the bandpass range.

Considering $\zeta_{active} = 0.7$, figure 5.9 shows overshoot percentage and settling time against frequency range [0.1 3] on a log scale. This plot can also be shown as overshoot percentage and settling time against the degree of phase at that frequency figure 5.10. Note that these plots cannot be superimposed directly as the frequency is expressed on the log scale in figure 5.9, and the phase is varied in absolutes in figure 5.10, but it

is understood that both plots are the same. From these plots, it is clear that in the region of phase lead, the performance is quite poor, but steadily improves as the phase reduces (natural frequency increases).

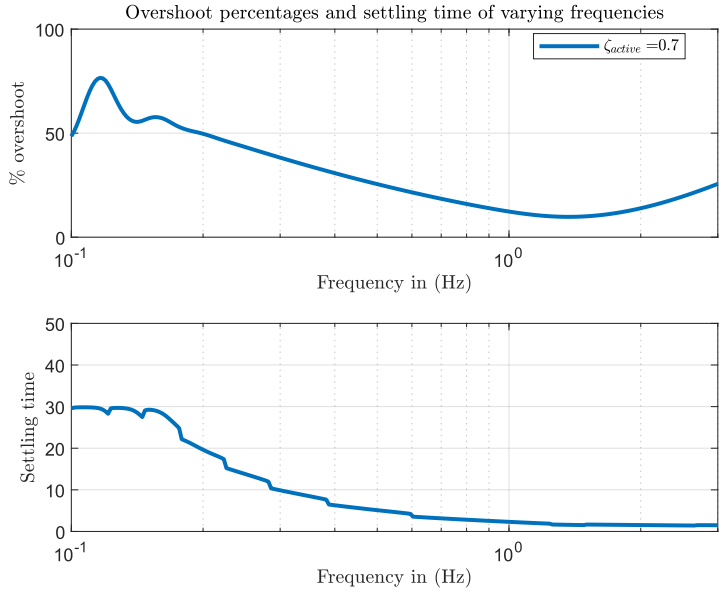

Figure 5.9: Overshoot percentage and settling time of varying plant resonance frequency in [0.1 3]Hz, when $\zeta_{active} = 0.7$. These characteristics also relate to the phase of $\mathscr{R}_{bp}$ at that frequency

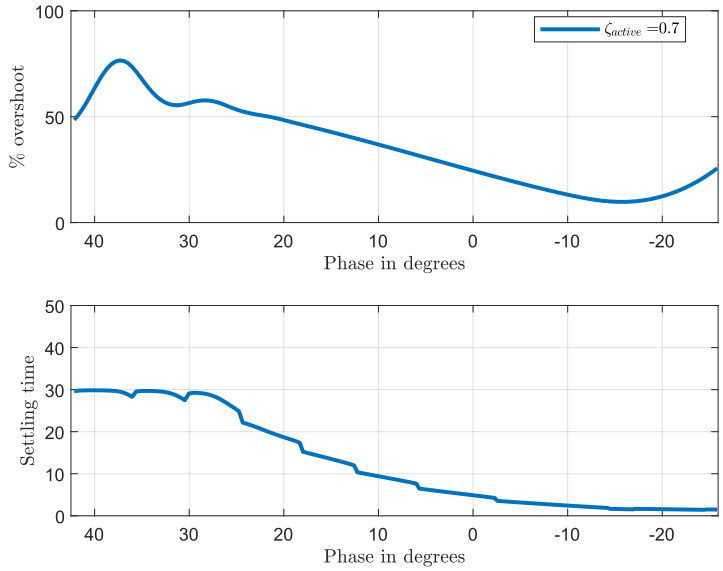

Figure 5.10: Overshoot percentage and settling time of a plant under a range of phase 43 to -25.8 degrees, when $\zeta_{active} = 0.7$. These are the phase values provided by $\mathscr{R}_{bp}$ at that particular frequency at which the plant has its resonance frequency.

To check how a change in damping gains would influence performance, a range of dimensionless active gains $\zeta_{active} \in [0.2\ 10]$ is selected and tested for this control setup (figure 5.11). Note that increase in damping gain makes the system overedamped, and increases the settling time and overshoot relatively. Apart from the fact that the plot is overloaded, a clear conclusion to the first question can be made - It is only for phase lower than 0 is when settling times are lower than 5 seconds with optimal overshoot percentages. Therefore, a phase lag is necessary after reset for improved performance.

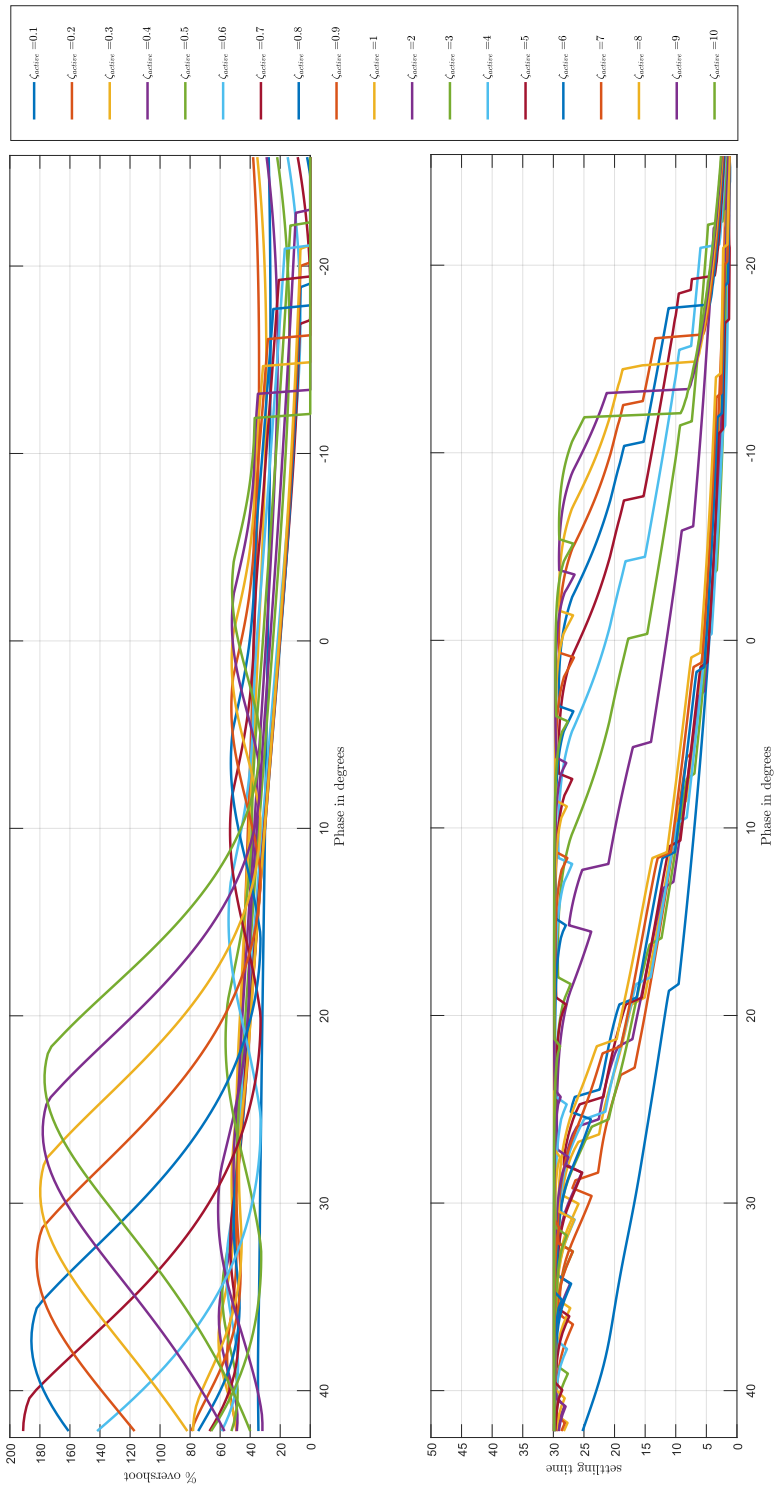

Figure 5.11: Overshoot and settling time over a range of active gains

For the second question, the plots are focused to the phase lag region. This is means the plant natural frequency should be within 1Hz-3Hz. To have more clarity on observations, the plots are split in 4 sets of active gains. Figures 5.12 and 5.13 show the performance when $\zeta_{active} \in [0.2\ 1]$. Figures 5.14 and 5.15 show the performance when $\zeta_{active} \in [1\ 10]$. As observed in the previous section, due to numerical and mathematical error, active damping gains from 1 to 5 have proven to be erroneous. The plots are shown merely for uniformity purposes, and no inferences are concluded from data of that range. It is very apparent that for a particular amount of ζ_{active}, as the phase reduces the performance improves to a point after which there is not overshoot observed, and settling times are very quick. One inference can be made that beyond that degree of phase, any more tuning is unnecessary because even if there is no overshoot present, settling times are reducing at a very low rate.
For example, the current designed controller $\mathscr{R}_{bp}$ provides a phase lag of 19.8 degrees for the natural frequency of the system used for simulations from [3]. Therefore for such a setup, the best choice of active gain would be 0.9 (as shown in figure 5.13), as this combination provides the most optimum overshoot percentage and fastest settling time.

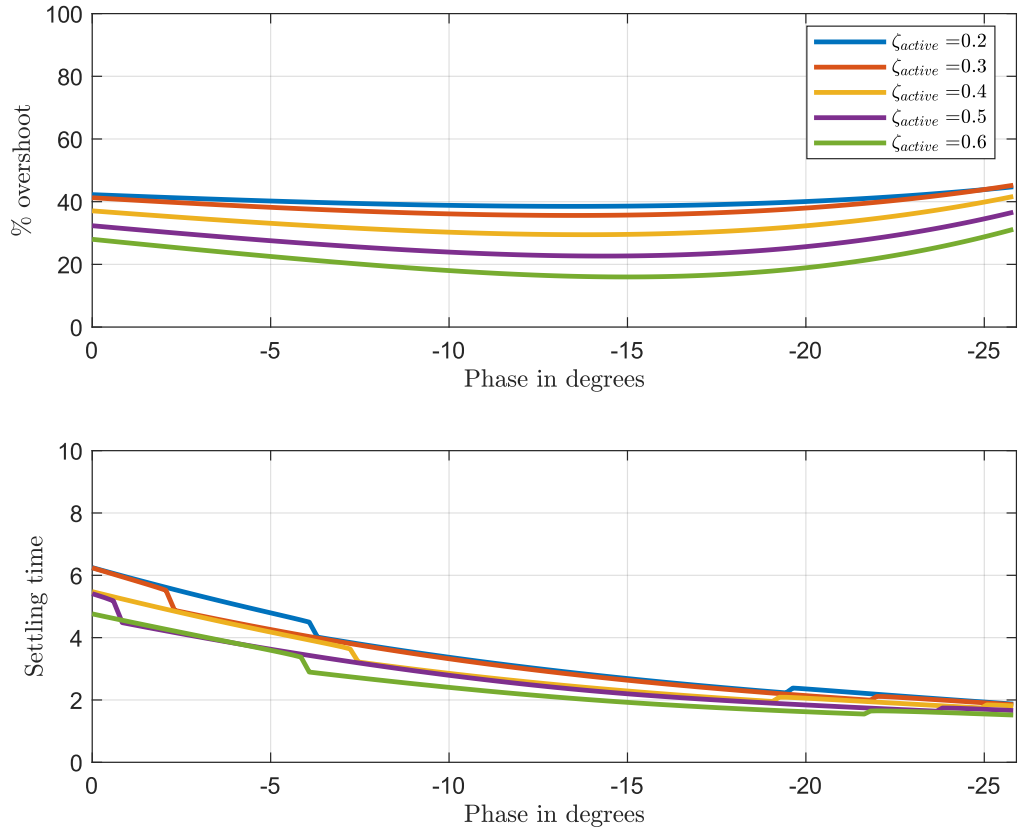

Figure 5.12: Overshoot percentage and settling time of a plant under a range of phase 0 to -28.5 degrees, with ζ_{active} ranging from 0.2 to 0.6.

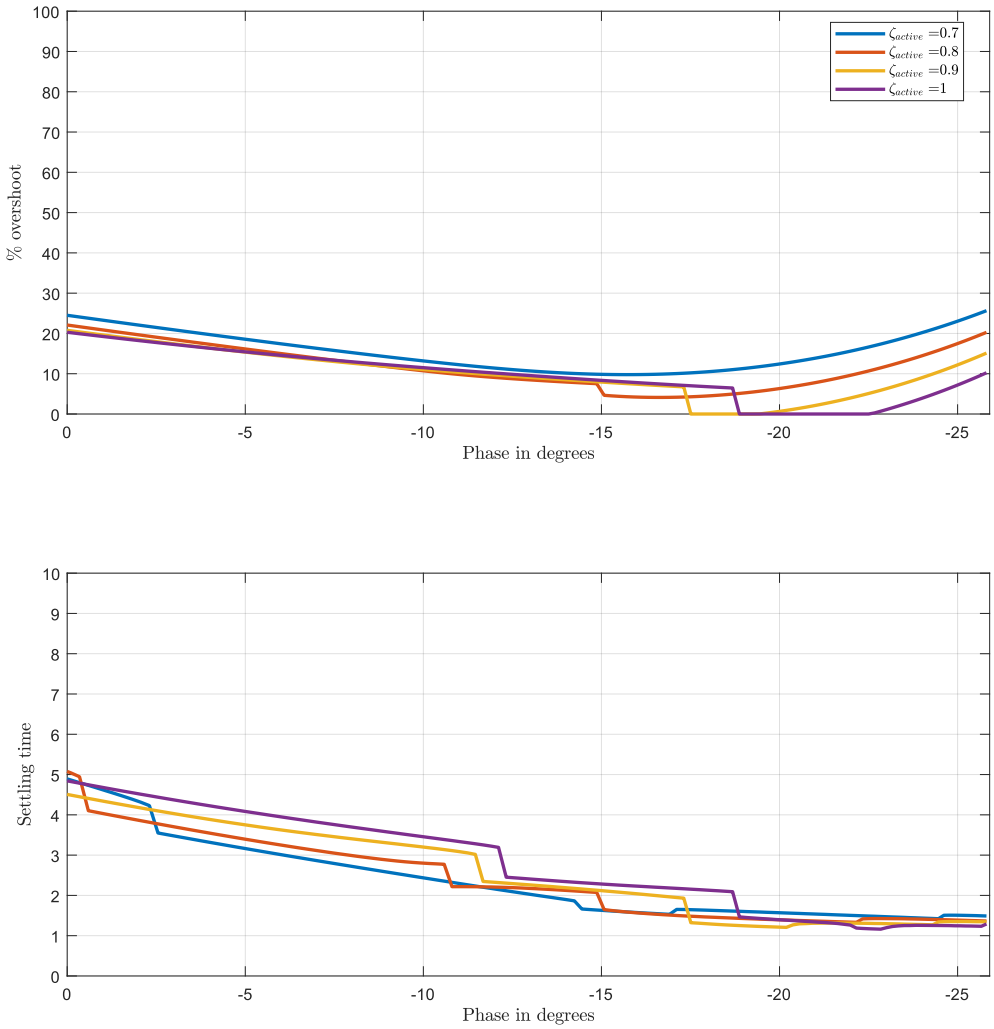

Figure 5.13: Overshoot percentage and settling time of a plant under a range of phase 0 to -28.5 degrees, with ζ_{active} ranging from 0.7 to 1.

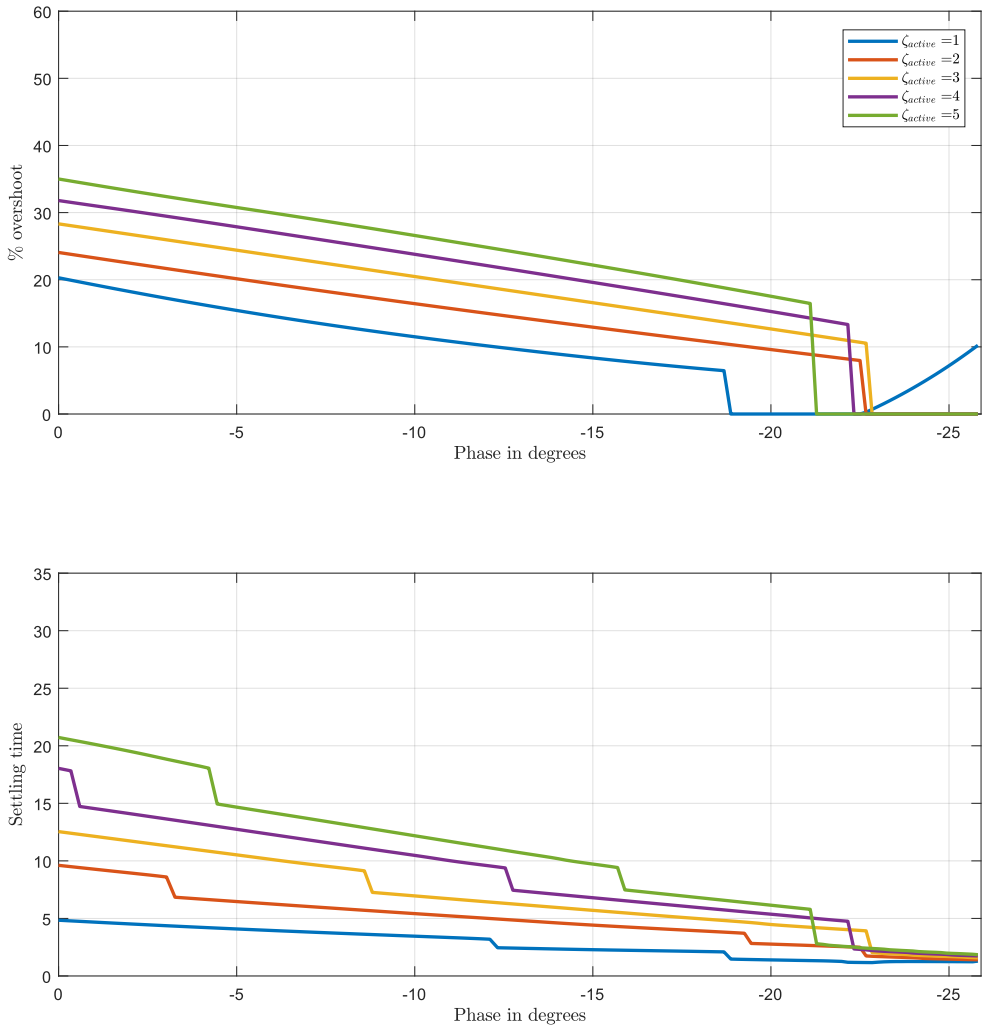

Figure 5.14: Overshoot percentage and settling time of a plant under a range of phase 0 to -28.5 degrees, with ζ_{active} ranging from 1 to 5.

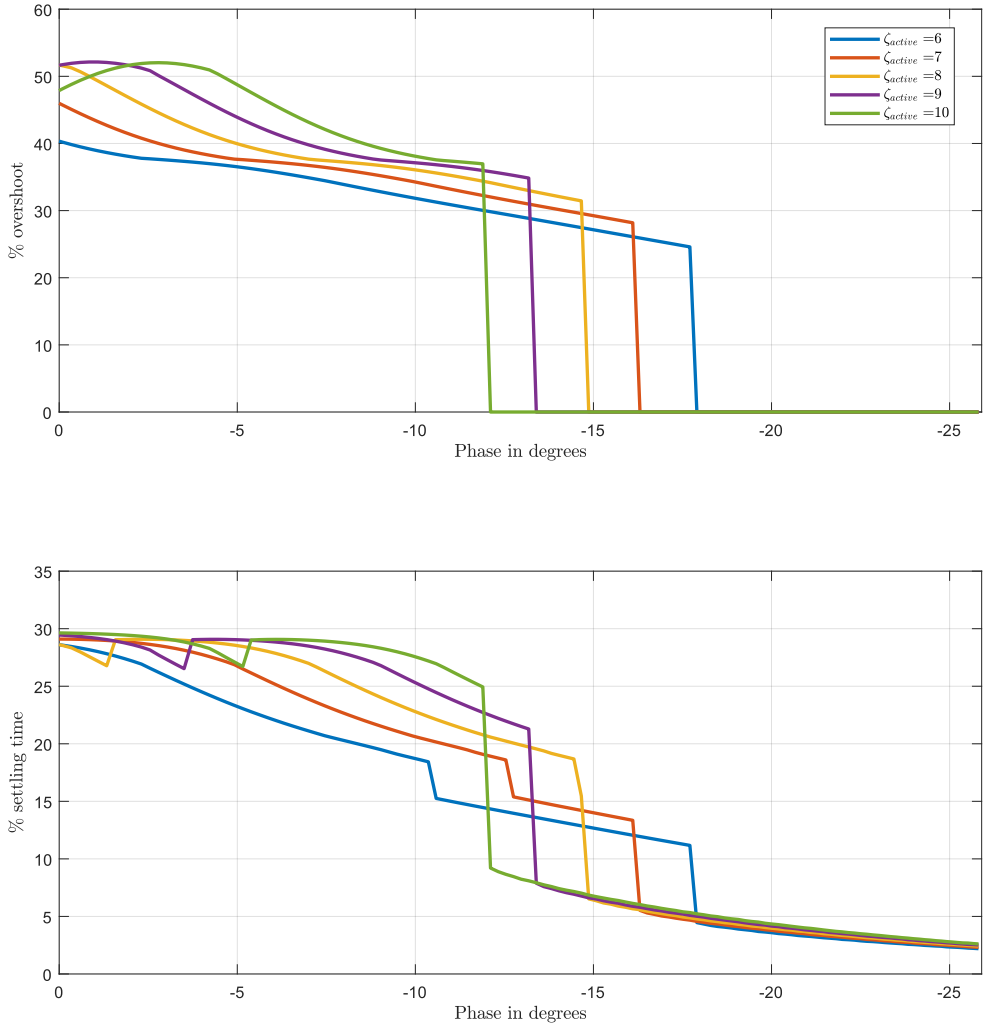

Figure 5.15: Overshoot percentage and settling time of a plant under a range of phase 0 to -28.5 degrees, with ζ_{active} ranging from 6 to 10.

5.4. High frequency oscillations early in the transient response at higher damping gains

It is also observed that in figure 5.2, as ζ_{active} increases, there are small but high frequency oscillations occurring at the start of the response. Although performance has greatly improved, there is still a need to address this anomaly. There can be two reasons for this, either the influence of higher order harmonics, or because the damping gain is more than necessary and reset is occurring prematurely. Since the anomaly happens after $\zeta_{active} = 1$, this value of active gain is selected for simulations.

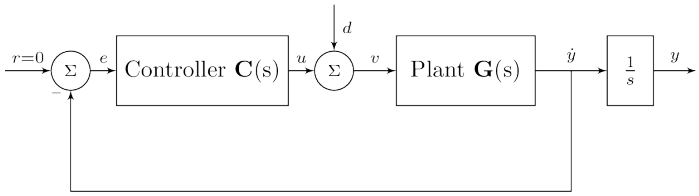

Figure 5.16: Block diagram of a motion control system. No reference is added as it is focusing strictly on disturbance rejection.

Figure 5.16 shows the control loop of the system, which will be used as a refernce to derive our open loop and closed loop equations. An open loop analysis is done before introducing feedback, the gain of which is given by the relation:

$$OL = G(s) \cdot C(s) \quad = G(s) \cdot \beta \cdot \mathscr{R}_{bp} \tag{5.1}$$

The controller transfer function, as explained towards the end of 2.1, consists of active damping gain β, and the gain provided by the designed bandpass filter $\mathscr{R}_{bp}$. Figure 5.17 shows clearly that there is influence due to higher order harmonics at lower frequencies. However, they are still in the designed band of $\mathscr{R}_{bp}$, which is a cause of concern.

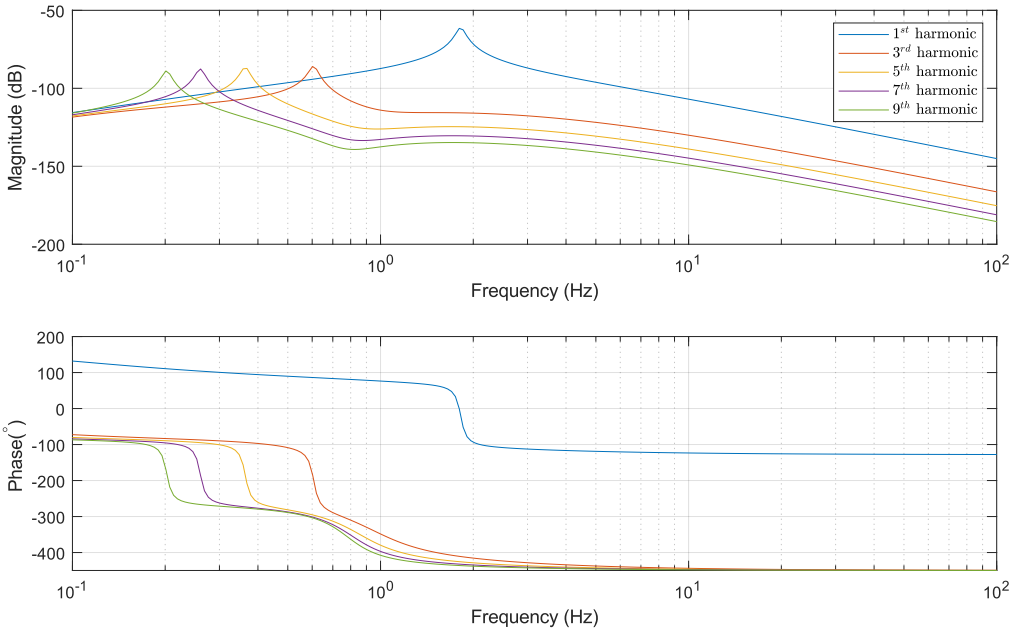

Figure 5.17: Plant+Controller Open loop and presence of higher order harmonics due to reset.

Closed loop analysis is done by making use of the gang of 4 [32], mainly the process sensitivity function shown below in equation 5.2

$$\frac{e}{d} = \frac{G(s)}{1 + G(s)C(s)} \tag{5.2}$$

Plotting closed loop DF's are still being researched in literature, and a very simplified algorithm is used from [12]. It is seen in figure 5.18 that the gain of the higher order harmonics is less than first order in the closed loop plot. They may have an influence in the closed loop, and should be checked with a better and accurate algorithm of the DF.

The next reasoning can be premature reset due to too much gain. Figure 5.19 shows a zoomed in shot of a step disturbance response to the system, when $\zeta_{active} = 10$. It can be clearly seen that there is a wave of oscillations at the start of the response. Also a small peak is seen as the first "overshoot". Systems operating

in a phase lag show slight instability at the start of a step response but eventually make it to the steady state. To check this we must check how the input and the output of the reset controller looks like in time domain, ie the velocity and the control force generated. Figures 5.20, 5.21, 5.22, 5.23 illustrate these parameters, and it is observed that at the first instance of reset (at 1.8 seconds), where the velocity crosses zero. It is observed that the velocity and control force amplitude's gradually decrease exponentially quicker than the linear counterpart, which explains the improved performance. However the cause of multiple resets is most likely related due to the incomplete storage of energy in the system. As discussed in section 2.3, reset based damping removes energy from the system and injects damping. Doing so prematurely will force the system to do a "discreet" step wise motion, making its way to steady state.

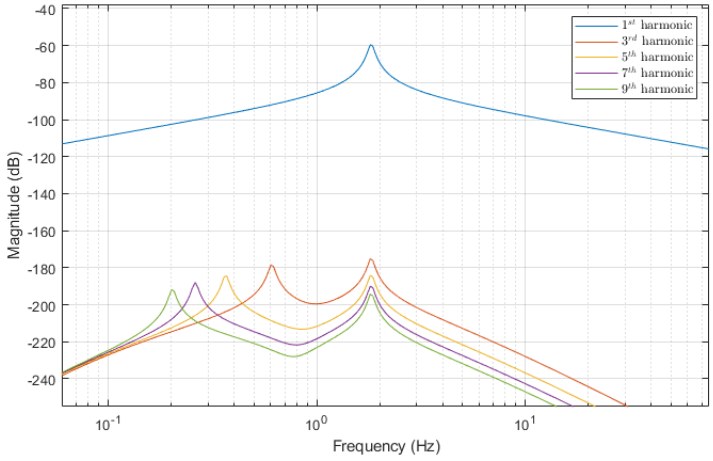

Figure 5.18: Plant + Controller Closed loop approximation DF showing the presence of higher order harmonics due to reset.

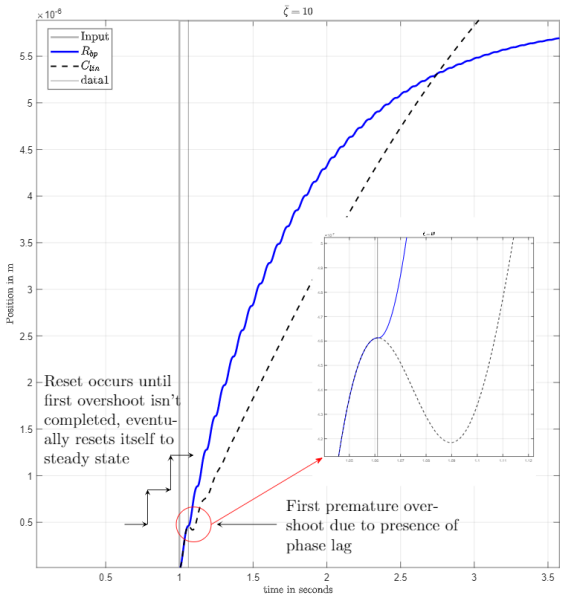

Figure 5.19: Multiple resets occurring for $\zeta_{active} = 10$. Mainly due to premature reset and incomplete initial "overshoot" due to the phase lag in the system.

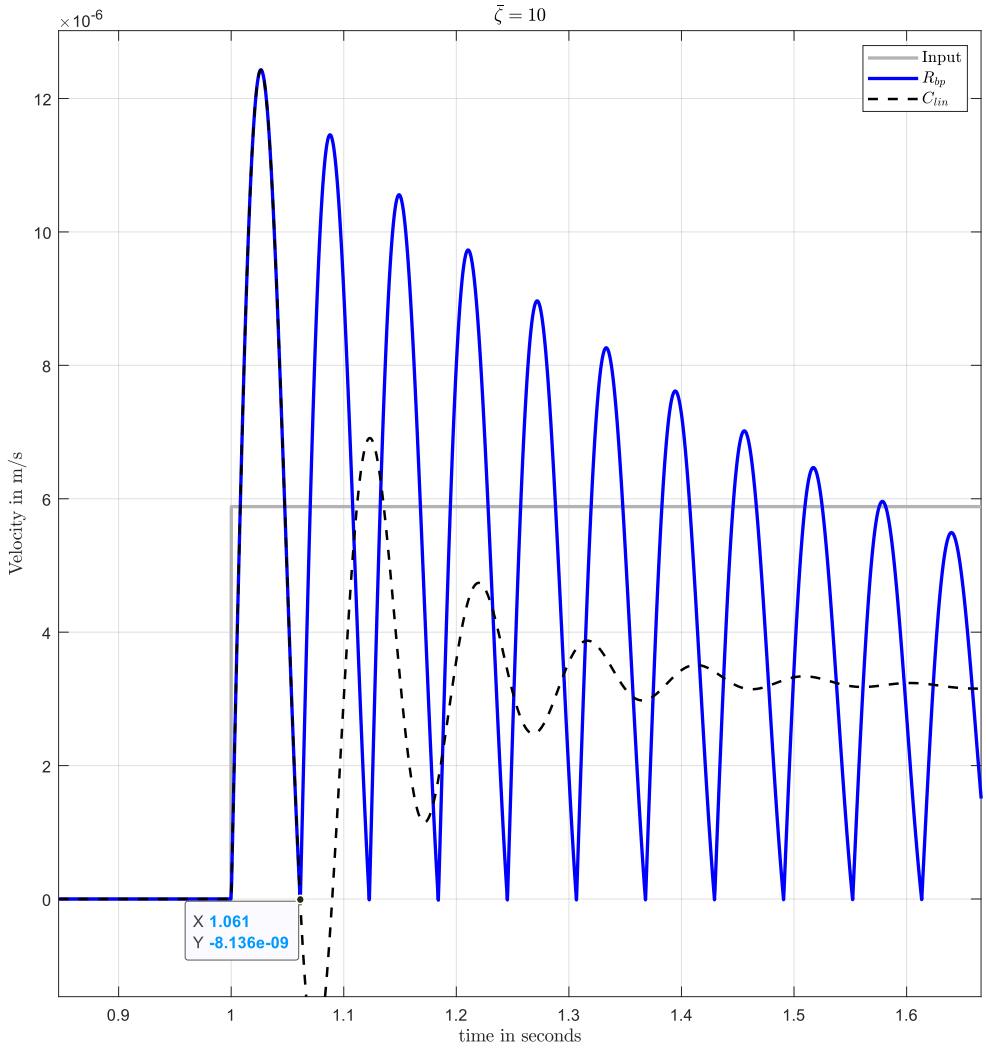

Figure 5.20: Velocity plot of the system being damped with $\zeta_{active} = 10$.

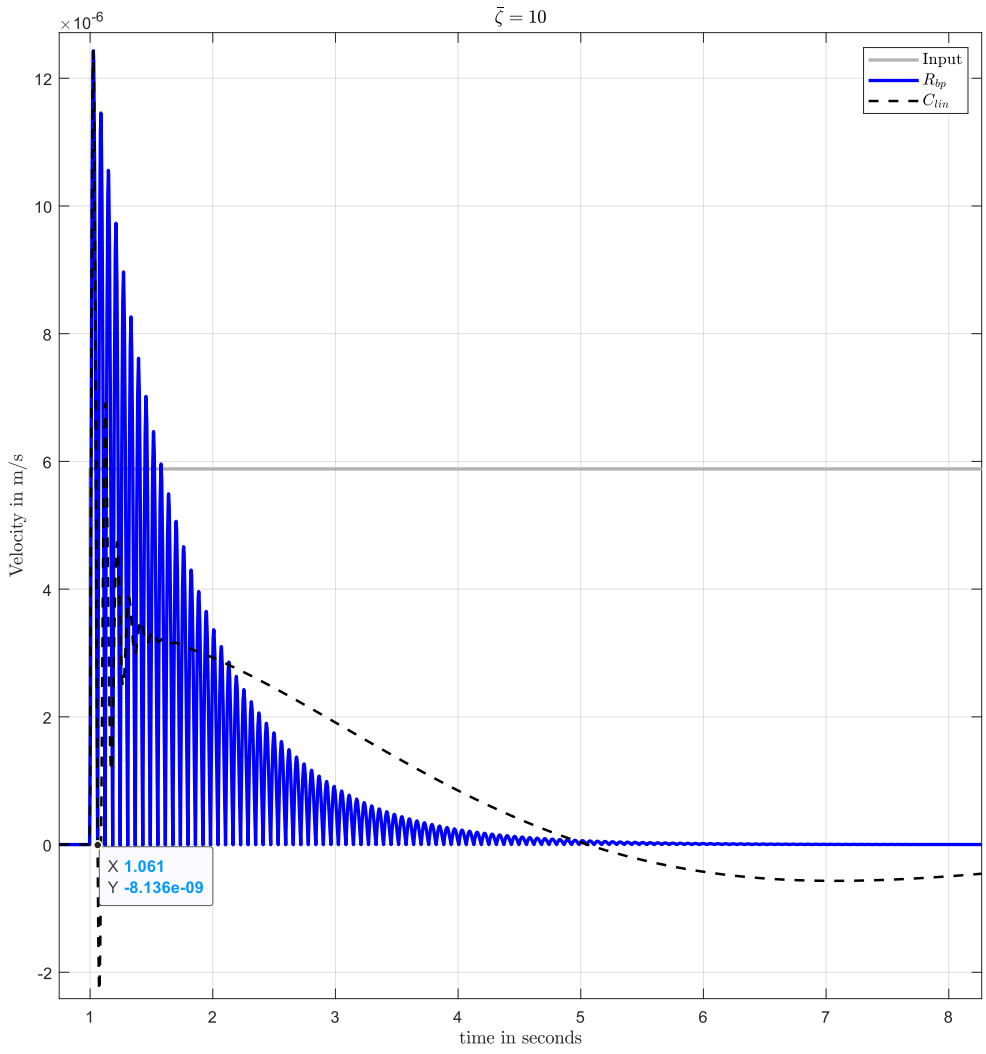

Figure 5.21: Velocity plot (Zoomed out) of the system being damped with $\zeta_{active} = 10$.

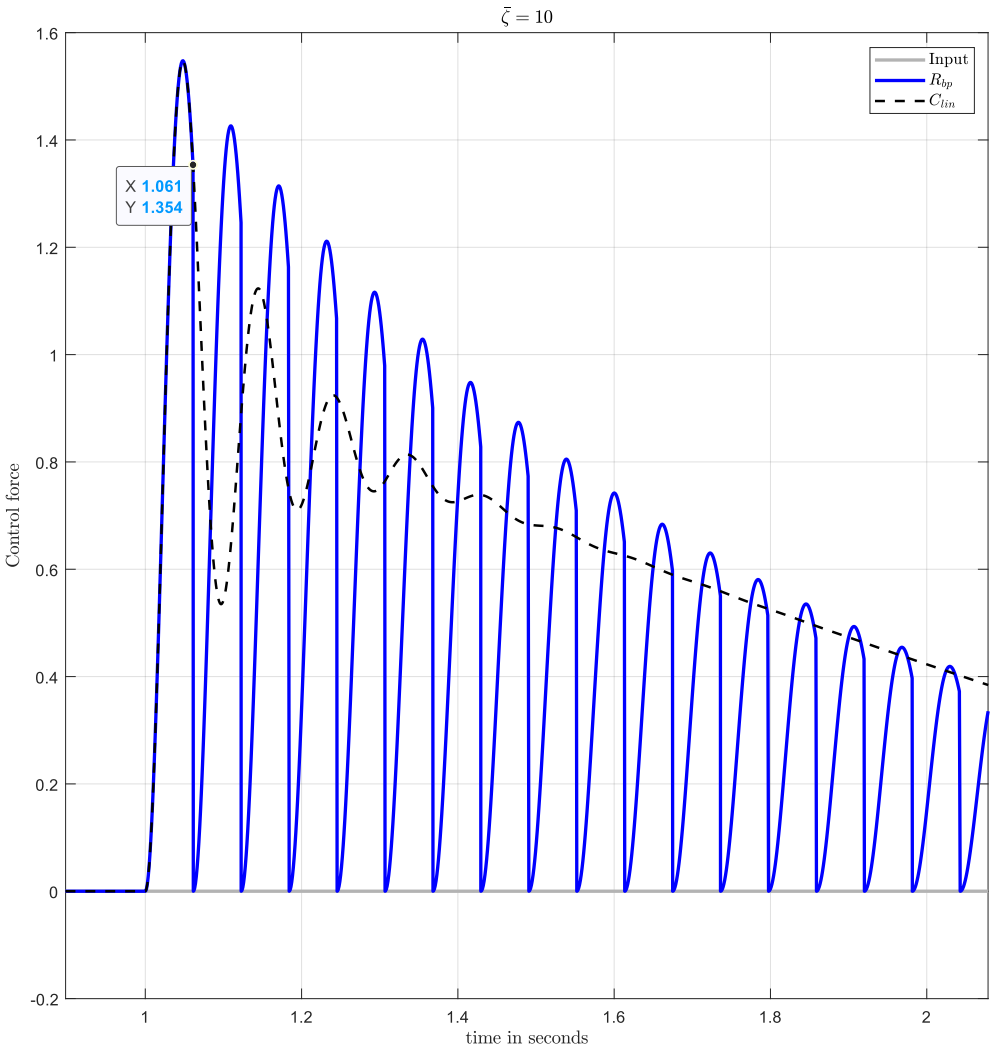

Figure 5.22: Control force plot of the system being damped with $\zeta_{active} = 10$.

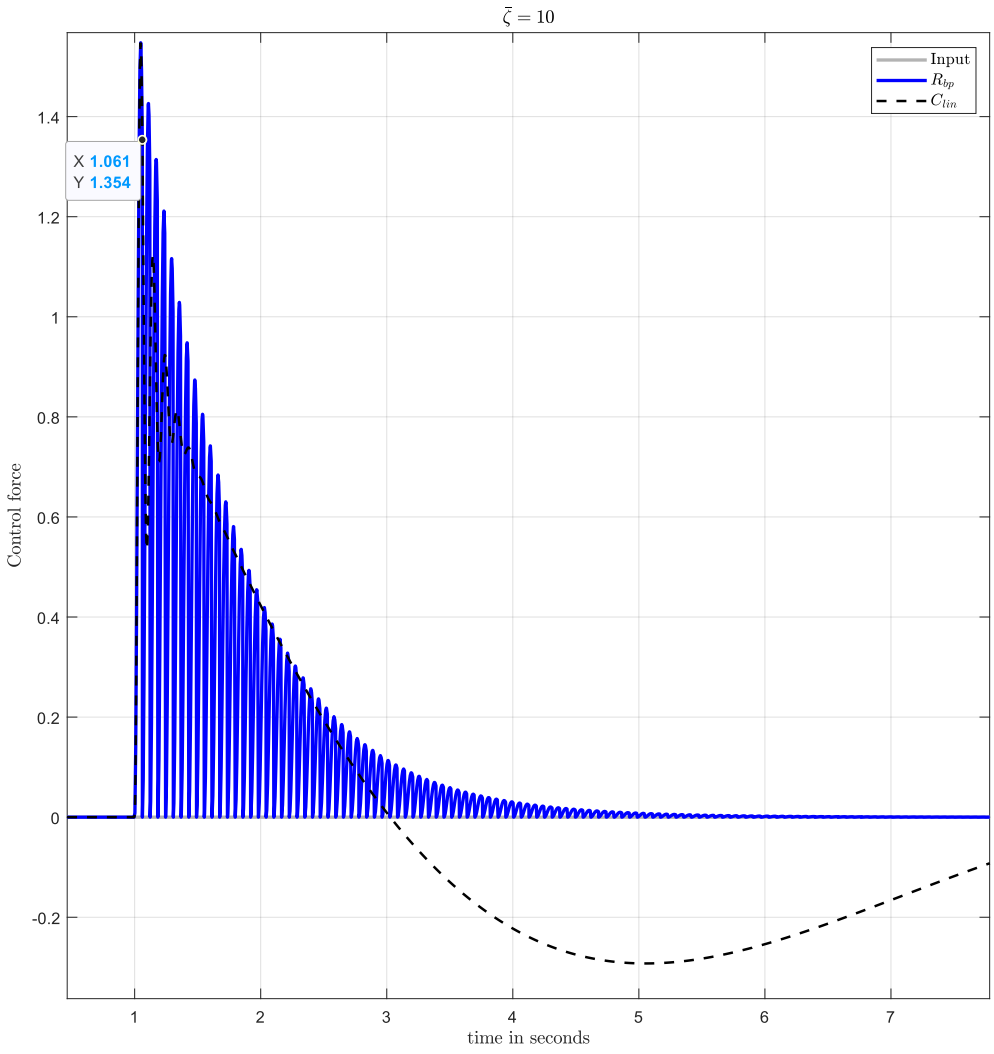

Figure 5.23: Control force (Zoomed out) plot of the system being damped with $\zeta_{active} = 10$.

6

Conclusion and Future recommendations

In this thesis, a novel control technique using nonlinear control methods was developed to improve transient characteristics when used as a skyhook damping controller. The motivation for this was to increase throughput in high-precision machines, which is limited due to structural or ambient vibrations.

After performing a literature survey of the state-of-the-art, linear active damping techniques proved to be lacking in terms of improvement and restricted by bodes sensitivity integral and the waterbed effect. Reset control - a form of nonlinear control technique- showed great potential to improve transient damping characteristics.
A controller was designed by having two fores in parallel and was numerically validated by using it on a real-time plant, the parameters of which have been taken from [3]. The plant model used is that of a metrology table provided by ASML at the Technical university of Eindhoven. The plant is tested using a step, impulse and sinusoidal disturbances, and has proven to provide over 70% reduction in settling time when compared to a linear bandpass for the same active control gain. The controller performs better than a linear bandpass even at lower damping gains, and the drawback of linear controllers at higher damping gains is overcome by substantially improved performance.
The controller operates in the presence of a certain phase lag, and it is concluded that for this architecture, a phase lag of 19.63 degrees is required at best at the resonance frequency. The controller will not perform at its best if the phase is in the positive, or above this value, and any further phase lag than is not necessary.

As future work, the following recommendations are proposed:

- The study can be extended by performing experimental validation of these results. There are numerical errors present at a particular range of gains, and this can be cleared out with experiments on the setup itself.
- The bandpass can be widened to attack multiple resonance modes at once. This research only focused on a band which is a decade long and focused on isolating vibrations on the first resonance mode of the system.
- Since a phase lag is necessary, having a constant phase lag throughout the bandpass could be tested for performance. There can also be an improvement to have a stable gain so that gain normalization is not required.
- Currently the controller is not explicitly designed to be robust to plant variations, and is an area of research which can be explored. Work is being done in the field of reset control to bandpass nonlinearities [24] of a reset based system. This needs to be done to reduce the influence of higher order harmonics in the open loop.
- The effects of external delays on the system has not been studied in this research, and should be explored to further test the phase lag operating condition of the controller.
- Stability analysis and an extensive closed loop analysis can be performed on the controller.

A

MATLAB Codes for Active isolation

https://drive.google.com/file/d/1v7ozAGZoRVWVvqhcrKM0HNDzH97RTFoF/view?usp=sharing

The above link contains a zip file with the following files.

- AVI_comparisiondata_plots.m - This file will help to retrace everything from the results chapter. It is one block of code containing different sections to plot the transient response to a step, impulse or a sinusoidal disturbance. The dimensionless active damping ratio $zeta_{active}$ can be varied as well, along with the plant natural frequency to test how it would respond in a varying degree of phase difference.
- AVI_parameters_export.slx - This file is the Simulink model of the controllers tested in a closed loop with a plant, along with input disturbances which can be changed accordingly. The file also contains a variety of scopes to check the process at a particular location of the loop.
- Controller_response_pg2.slx - This file is the Simulink model for only testing controller responses in open loop, and is made to easily compare with alternative controllers.
- hosidf.m - The HOSIDF plotting code. It's input are the state-space variables of the system being reset [A ,B, C, D], the reset matrix A_r, the order of harmonics activated to be shown, a frequency range in logspace, choice to hold the plot, and the dimension of input frequency (Hz or rad/sec).
- hosidfcalc.m - The mathematical model which calculates the order of harmonics, based on [19] [13] [15] [27].
- ssdatacanonicalform.m - A code which converts a transfer function to its state-space variables in the canonical form.

Bibliography

[1] WHTM Aangenent et al. “Performance analysis of reset control systems”. In: *International Journal of Robust and Nonlinear Control* 20.11 (2010), pp. 1213–1233.

[2] S.P. Achten. “HIGS-based Skyhook damping design of a Multivariable Vibration Isolation System”. In: (2020).

[3] MA Beijen. “Disturbance feedforward control for vibration isolation systems: analysis, design, and implementation”. In: (2018).

[4] Michiel A Beijen et al. “Mixed feedback and feedforward control design for multi-axis vibration isolation systems”. In: *Mechatronics* 61 (2019), pp. 106–116.

[5] Orhan Beker et al. “Fundamental properties of reset control systems”. In: *Automatica* 40.6 (2004), pp. 905–915.

[6] Robert T Bupp et al. “Resetting virtual absorbers for vibration control”. In: *Journal of Vibration and Control* 6.1 (2000), pp. 61–83.

[7] RT Bupp et al. “Finite settling time control of the double integrator using a virtual trap-door absorber”. In: *Proceeding of the 1996 IEEE International Conference on Control Applications IEEE International Conference on Control Applications held together with IEEE International Symposium on Intelligent Contro*. IEEE. 1996, pp. 179–184.

[8] JC Clegg. “A nonlinear integrator for servomechanisms”. In: *Transactions of the American Institute of Electrical Engineers, Part II: Applications and Industry* 77.1 (1958), pp. 41–42.

[9] Christophe Collette, Stef Janssens, and Kurt Artoos. “Review of active vibration isolation strategies”. In: *Recent patents on Mechanical engineering* 4.3 (2011), pp. 212–219.

[10] Consultancy.eu. *Global chip shortage costs automotive sector €90 billion*. URL: https://www.consultancy.eu/news/6273/global-chip-shortage-costs-automotive-sector-90-billion. (accessed: 01.09.2021).

[11] DA Deenen et al. “Hybrid integrator design for enhanced tracking in motion control”. In: *2017 American Control Conference (ACC)*. IEEE. 2017, pp. 2863–2868.

[12] Shrinath Diwakar. “Avoiding excessive zero crossings in reset control”. In: (2021).

[13] Yuqian Guo, Youyi Wang, and Lihua Xie. “Frequency-domain properties of reset systems with application in hard-disk-drive systems”. In: *IEEE Transactions on Control Systems Technology* 17.6 (2009), pp. 1446–1453.

[14] Yuqian Guo, Lihua Xie, and Youyi Wang. *Analysis and design of reset control systems*. Vol. 2. Iet, 2015.

[15] Yuqian Guo et al. “Optimal reset law design of reset control systems with application to HDD systems”. In: *Proceedings of the 48h IEEE Conference on Decision and Control (CDC) held jointly with 2009 28th Chinese Control Conference*. IEEE. 2009, pp. 5287–5292.

[16] M.F. Heertjes et al. “Experimental evaluation of reset control for improved stage performance”. English. In: *IFAC-PapersOnLine* 49.13 (2016). 12th IFAC Workshop on Adaptation and Learning in Control and Signal Processing (ALCOSP 2016), ALCOSP 2016 ; Conference date: 29-06-2016 Through 01-07-2016, pp. 93–98. ISSN: 2405-8963. DOI: 10.1016/j.ifacol.2016.07.933.

[17] Marcel Heertjes et al. “Hybrid integrator-gain system for active vibration isolation with improved transient response”. English. In: *IFAC-PapersOnLine* 52.15 (Sept. 2019), pp. 454–459. ISSN: 2405-8963. DOI: 10.1016/j.ifacol.2019.11.717.

[18] Marcel F Heertjes et al. “Switching control in vibration isolation systems”. In: *IEEE Transactions on Control Systems Technology* 21.3 (2012), pp. 626–635.

[19] Kars Heinen. “Frequency analysis of reset systems containing a Clegg integrator: An introduction to higher order sinusoidal input describing functions”. In: (2018).

[20] Isaac Horowitz and Patrick Rosenbaum. “Non-linear design for cost of feedback reduction in systems with large parameter uncertainty”. In: *International Journal of Control* 21.6 (1975), pp. 977–1001.

[21] Klaus Janschek. *Mechatronic systems design: methods, models, concepts*. Springer Science & Business Media, 2011.

[22] N. Karbasizadeh et al. “Benefiting from Linear Behaviour of a Nonlinear Reset-Based Element at Certain Frequencies”. In: *2020 Australian and New Zealand Control Conference (ANZCC)* (2020), pp. 226–231.

[23] Nima Karbasizadeh, Niranjan Saikumar, and S Hassan HosseinNia. “Fractional-Order Single State Reset Element”. In: ().

[24] Nima Karbasizadeh et al. “Band-Passing Nonlinearity in Reset Elements”. In: *arXiv preprint arXiv:2009.06091* (2020).

[25] Sang-Myeong Kim and Jae-Eung Oh. “A modal filter approach to non-collocated vibration control of structures”. In: *Journal of Sound and Vibration* 332.9 (2013), pp. 2207–2221.

[26] KR KRISHNAN and IM HOROWITZ. “Synthesis of a non-linear feedback system with significant plant-ignorance for prescribed time-domain tolerances(Design of nonlinear feedback system with significant plant ignorance for prescribed time domain tolerances)”. In: (1973).

[27] Ying Li, Guoxiao Guo, and Youyi Wang. “Nonlinear mid-frequency disturbance compensation in hard disk drives”. In: *IFAC Proceedings Volumes* 38.1 (2005), pp. 31–36.

[28] Peng Lu, Timothy Sandy, and Jonas Buchli. “Adaptive Unscented Kalman Filter-based Disturbance Rejection With Application to High Precision Hydraulic Robotic Control”. In: *2019 IEEE/RSJ International Conference on Intelligent Robots and Systems (IROS)*. IEEE. 2019, pp. 4365–4372.

[29] André Preumont. *Vibration control of active structures: an introduction*. Vol. 246. Springer, 2018.

[30] Christophe Prieur et al. “Analysis and synthesis of reset control systems”. In: *Foundations and Trends in Systems and Control* 6.2-3 (2018), pp. 117–338.

[31] N. Saikumar, R. K. Sinha, and S. H. HosseinNia. ““Constant in Gain Lead in Phase” Element– Application in Precision Motion Control”. In: *IEEE/ASME Transactions on Mechatronics* 24.3 (2019), pp. 1176–1185. DOI: 10.1109/TMECH.2019.2909082.

[32] R Munnig Schmidt, Georg Schitter, and Adrian Rankers. *The design of high performance mechatronics-: high-Tech functionality by multidisciplinary system integration*. Ios Press, 2020.

[33] Gunter Stein. “Respect the unstable”. In: *IEEE Control systems magazine* 23.4 (2003), pp. 12–25.

[34] SJLM Van Loon et al. “Frequency-domain tools for stability analysis of reset control systems”. In: *Automatica* 82 (2017), pp. 101–108.

[35] Wallace E Vander Velde et al. “Multiple-input describing functions and nonlinear system design”. In: *McGraw lill* (1968).

[36] Jinchuan Zheng et al. “Improved reset control design for a PZT positioning stage”. In: *2007 IEEE International Conference on Control Applications*. IEEE. 2007, pp. 1272–1277.